Dynamic polarization of graphene by external correlated charges

I. Radović and D. Borka

VINČA Institute of Nuclear Sciences, University of Belgrade, P.O. Box 522, 11001 Belgrade, Serbia

Z. L. Mišković[*]

Department of Applied Mathematics, and Waterloo Institute for Nanotechnology, University of Waterloo, Waterloo, Ontario, Canada N2L 3G1

We use the dielectric response formalism within random phase approximation for graphene's π-electron bands to study polarization of doped, single-layer graphene in the presence of a moving dipole and a pair of comoving ions, as well as to study the electrostatic part of the long-range interaction in the coadsorption of two ions and two dipoles on graphene. We find that the vector components of both the force and the torque on the moving dipole include both the conservative and dissipative contributions, whereas the wake in the induced charge density in graphene shows asymmetry with respect to the direction of dipole's motion. Furthermore, the screened interaction energy between two comoving ions shows oscillations as a function of the interionic separation that may give rise to a wake-riding bound state of the ions, whereas the total energy loss of those ions shows both constructive and destructive interference effects in comparison with the energy loss of independent ions. In the case of static coadsorption on doped graphene, strong screening of the ion-ion electrostatic interaction energy is found as a function of their separation, whereas antiscreening is found in the interaction energy between two dipoles having dipole moments perpendicular to graphene. In addition, shallow minima are found in the interaction energies at finite separations between two ions and between two dipoles having dipole moments parallel to graphene due to Friedel oscillations, which are shown to be much weaker than in the case of coadsorption on a comparable two-dimensional electron gas with single parabolic energy band. It is shown that the interaction of graphene with all the above model systems may be effectively controlled by changing the doping density of graphene.

PACS number(s): 73.22.Pr, 79.20.Rf

I. INTRODUCTION

Recent reviews of the charge carrier transport and other properties of graphene's π-electron bands emphasized the importance of their interaction with charged impurities, which may be trapped in a substrate or directly adsorbed on graphene.[1,2] In particular, it was shown recently that spatial correlation among static charged impurities may explain several intriguing properties observed in the conductivity of single-layer graphene.[3,4] In that context, formation of clusters, or islands of atoms adsorbed on graphene, may also strongly affect the mobility of charge carriers in graphene.[5] On the other hand, the structure of the adsorbate assemblies on graphene at submonolayer coverages is expected to depend on the interaction energy between adatoms or admolecules, which is, in turn, affected by the ability of graphene's π electrons to screen the electrostatic part of that interaction. Such substrate-mediated interaction is known to play a key role in the coadsorption phenomena on solid surfaces.[6] For example, metal surfaces that support a surface state characterized by two-dimensional electron gas (2DEG) with parabolic energy dispersion were shown to exhibit Friedel oscillations (FOs), which may be used to discuss the ordering phenomena in the adsorbed submonolayers of ionized atoms[7,8] and dipolar molecules.[9]

In the case of adsorption on graphene, the possibility to control its equilibrium charge carrier density n by capacitive gating or by direct charge transfer from the adsorbed atoms offers an interesting means of controlling the long-ranged electrostatic interaction between the adatoms via changing the screening ability of graphene. Such a mechanism should work well for adsorbates that do not hybridize with graphene's

π-electron bands,[10] such as alkali atoms that form ionic bond with graphene,[11] or for closed-shell adsorbates that are characterized by a large dipole moment, such as water molecules.[12] With the spatial correlation among adsorbed species being essentially determined by the screened interaction between them, one could devise an effective way of controlling the mobility of charge carriers in graphene, as was shown in the case of controlled K-atom adsorption on free-standing graphene.[13] Of course, the role of substrate should also be taken into account in such processes because of the presence of uncontrolled amount of trapped charges.[2,14]

However, there are only few recent experimental studies of structure and dynamics of submonolayer assemblies of adatoms of relevance to graphene, examining the diffusion of the K atoms on graphite[15] and formation of the Cs superlattices on graphene.[16] Noting that the alkali adatoms are largely ionized due to charge transfer to graphene, those studies demonstrated the existence of a strong dipole-dipole–like repulsion between the adatoms that prevents cluster formation. However, no conclusive evidence was found of ordering that may result from the long-ranged FOs in the adatom interaction energy on graphene,[15,16] which is in contrast to the observations on metallic surfaces with 2DEG.[7–9] A possible explanation may come from the fact that the amplitude of FOs in graphene decays faster than their amplitude in 2DEG.[17–19] Furthermore, studying the electrostatic dipole-dipole interactions on graphene may also be of interest for, e.g., extending the studies of relaxation dynamics of liquids near nonmetallic surfaces,[20] formation of a superlattice in an assembly of nanoparticles on graphitic surfaces,[21] or electrostatic modeling of lateral interactions between polar molecules adsorbed on metal surfaces.[22]

On the other hand, interactions of graphene with external charges that move at the speed on the order of graphene's π-band Fermi speed v_F ($\approx c/300$, with c being the speed of light in vacuum) were recently studied experimentally in the context of both the high-resolution reflection electron energy-loss spectroscopy (HREELS) (Refs. [23]–[26]) and the low-energy scattering of the Li and H ions.[27,28] In the theoretical accounts of such interactions, dynamic polarization of graphene's π-electron bands was described by a kinetic model[29] and by a dielectric function within the random phase approximation (RPA),[18,30–32] including the damping effects via Mermin's approach,[33] local-field effects,[34,35] and the coupling with substrate phonons.[34,36,37] It was shown that graphene exhibits important differences with respect to a 2DEG (Refs. [38] and [39]) in both the stopping (dissipative) force and the image (conservative) force, as well as in the wake effect in the induced charge density in graphene due to a moving point charge,[35] which arise mostly due to the effects of graphene doping and the role played by the interband single-particle excitations (SPEs).[40]

In the above studies, particular attention was paid to the interaction with charged particles moving parallel to graphene,[29,33,41,42] of relevance for possible extensions of the ion-surface grazing scattering technique to graphene,[43–45] as well as for channeling of fast ions[46–52] and molecules[53,54] through carbon nanostructures. In that context, motivated by observations made in the scattering of molecules on solid surfaces[55–57] and in the channeling of molecules through carbon nanotubes,[53] it is worthwhile exploring the phenomenology that may arise in grazing scattering of the molecular projectiles from graphene. Such processes may include the dissociation of the incident molecule,[58,59] Coulomb explosion of its ionic fragments,[60,61] vicinage effect in the energy loss of these fragments,[62] secondary electron emission from the surface,[57] and the radially constrained oscillations of ion fragments in nanotubes.[53] It is also of interest to study the interaction of graphene with fast, undissociated molecules with permanent electric dipole moment, in analogy with the studies of grazing scattering of a dipole from a metal surface[63] or supported 2DEG,[64] and channeling of a dipole through a carbon nanotube.[54] Moreover, investigation of the dissipative processes occurring due to the dynamic Casimir interaction between slow dipolar molecules with metal surfaces has received considerable attention recently,[65–67] which renders studying such processes on graphene also worthwhile.

With a view to such applications, we study the interaction of graphene with multiple point charges representing ions that move in a correlated manner over graphene, as would occur in Coulomb explosion of molecular or cluster projectiles, as well as with point dipoles representing undissociated molecules or atoms with permanent dipole moment that may be regarded as a limiting case of closely correlated charges of opposite sign. In doing so, we consider a single-layer graphene and note that the use of the dielectric function within the RPA for its π electrons is justified for particles moving at distances z_0 above graphene that are larger than its lattice constant $a \approx 2.46$ Å (thereby neglecting the size of graphene's π-electron orbitals) with speeds satisfying the condition $v < 2z_0\varepsilon_c/\hbar$, where $\varepsilon_c \approx 1$ eV is a high-energy cutoff validating the approximation of linearized π-electron

bands (thereby neglecting the intervalley scattering of charge carriers in graphene).[18,32,33] When the projectile speed is normalized by the Fermi speed of graphene, the latter condition amounts to $v/v_F \lesssim 0.3 z_0$ with z_0 expressed in angstroms.

Our formulation of the problem readily takes into account the effects of substrate that supports dynamic polarization modes of its own and is placed a finite distance h underneath graphene, as well as the effects of damping and the local fields in graphene. However, our primary focus is to explore the effects of finite-equilibrium charge carrier density n in free-standing graphene, as well as the effects of the projectiles' speed v and its distance z_0 above graphene on (a) dissipative and conservative forces and torque on a moving dipole, (b) wake in the charge density in graphene induced by the moving dipole, (c) dynamically screened interaction energy between two comoving ions as a function of their separation d, and (d) correlated energy loss of two comoving ions. In the static limit, special attention is paid to the role played by FOs in the interaction energy between two ions and between two dipoles, coadsorbed on graphene. In addition, several comparisons are made with a "massive" 2DEG (m2DEG), characterized by a single parabolic energy band of relevance to metallic surface states, with its dielectric response also described within the RPA.[68] We note that, while several comments are specifically made on the results for intrinsic, or neutral ($n = 0$) graphene, one expects strong influence of the electron-hole puddles in this regime,[14] requiring a treatment that goes beyond present context.

After outlining the theoretical model in the next section, the presentation of the results is organized by first discussing a moving point dipole, followed by a discussion of the static limit for two particles, and concluded by considering a moving ion pair, whereas our conclusions will be summarized in the final section. In the Appendix, we outline a theory used for studying the wake effect in the induced charge density in graphene. Note that we use Gaussian electrostatic units, unless otherwise explicitly stated.

II. THEORY

We use a Cartesian coordinate system with coordinates $\mathbf{R} = \{\mathbf{r}, z\}$, where $\mathbf{r} = \{x, y\}$, and assume that graphene is placed in the $z = 0$ plane. A semi-infinite substrate with the (relative) dielectric constant ϵ_{sub} is assumed to occupy the region $z \leqslant -h < 0$ underneath graphene, while the region $z > -h$ is assumed to be vacuum or air. By performing the Fourier transform (FT) with respect to the coordinates parallel to graphene ($\mathbf{r} \rightarrow \mathbf{q}$) and with respect to time ($t \rightarrow \omega$), one may easily show that the screened interaction above graphene,[69] or the Green's function of the Poisson equation for this system $G(\mathbf{R},\mathbf{R}';t-t') \equiv G(\mathbf{r}-\mathbf{r}',z,z';t-t')$ for $z > 0$ and $z' > 0$, has its FT given by $\widetilde{G}(\mathbf{q},z,z';\omega) = \widetilde{G}_C(q,z,z') + \widetilde{G}_{\text{ind}}(\mathbf{q},z,z';\omega)$, where $\widetilde{G}_C(q,z,z') = (2\pi/q)e^{-q|z-z'|}$ corresponds to the bare Coulomb interaction, and

$$\widetilde{G}_{\text{ind}}(\mathbf{q},z,z';\omega) = \frac{2\pi}{q}e^{-q(z+z')}\left[\frac{1}{\epsilon(q,\omega)} - 1\right] \quad (1)$$

corresponds to the induced interaction due to polarization of graphene and the substrate. Here, the dielectric function of the

system is given by

$$\epsilon(q,\omega) = \epsilon_{\text{bg}}(q,\omega) + V_{\text{C}}(q)\Pi(q,\omega), \tag{2}$$

where $V_{\text{C}}(q) = 2\pi e^2/q$, and $\Pi(q,\omega)$ is the polarization function of noninteracting π electrons in free graphene.[18,30–32] In Eq. (2), the background dielectric constant is given by[69]

$$\epsilon_{\text{bg}}(q,\omega) = \left[1 - \frac{\epsilon_{\text{s}}(q,\omega) - 1}{\epsilon_{\text{s}}(q,\omega) + 1} e^{-2qh}\right]^{-1}, \tag{3}$$

corresponding to a substrate with nonlocal dielectric function ϵ_{sub} that depends on a three-dimensional (3D) wave vector $\{\mathbf{q}, q_z\}$ with $\mathbf{q} = \{q_x, q_y\}$ and on frequency ω, which yields within the specular-reflection model[34,69]

$$\epsilon_{\text{s}}(q,\omega) = \left[\frac{q}{\pi} \int_{-\infty}^{\infty} \frac{dq_z}{q^2 + q_z^2} \epsilon_{\text{sub}}^{-1}\left(\sqrt{q^2 + q_z^2}, \omega\right)\right]^{-1}, \tag{4}$$

where $q = \sqrt{q_x^2 + q_y^2}$. Note that, in a local approximation, the substrate is simply described by a frequency-dependent dielectric function giving $\epsilon_{\text{s}}(\omega) \equiv \epsilon_{\text{sub}}(\omega)$ in Eq. (4), as in the case of, e.g., strongly polar substrate that exhibits surface phonon modes.[34,37]

We further assume that a distribution of N-point particles, each carrying a charge $Z_j e$ (where $e > 0$ is the proton charge) and a dipole moment $\boldsymbol{\mu}_j$ with $j = 1, 2, \ldots, N$ is described by a charge density $\rho(\mathbf{R},t) = \rho_0(\mathbf{r} - \mathbf{v}t, z)$, which corresponds to a static distribution of charges with density $\rho_0(\mathbf{r}, z)$ defined in a frame of reference that moves rigidly with a velocity $\mathbf{v}$ parallel to graphene. This situation may correspond to a distribution of ionic fragments (with $\boldsymbol{\mu}_j = \mathbf{0}$) resulting from a Coulomb explosion of a cluster grazingly scattered from graphene, where the relative motion of the fragments with respect to each other may be treated as adiabatic within the moving frame of reference.[57] Denoting the position of the jth particle in that frame by $\mathbf{R}_j = \{\mathbf{r}_j, z_j\}$ with $z_j > 0$, we may write

$$\rho_0(\mathbf{r}, z) = \sum_{j=1}^{N} (Z_j e - \boldsymbol{\mu}_j \cdot \nabla_{\mathbf{R}}) \delta(\mathbf{R} - \mathbf{R}_j), \tag{5}$$

where $\delta(\mathbf{R} - \mathbf{R}_j) = \delta(\mathbf{r} - \mathbf{r}_j)\delta(z - z_j)$ is a 3D delta function. Therefore, with the induced potential in the region above graphene ($z > 0$) given by

$$\Phi_{\text{ind}}(\mathbf{R},t) = \int d^3\mathbf{R}' \int_{-\infty}^{\infty} dt' \, G_{\text{ind}}(\mathbf{R},\mathbf{R}'; t - t')\rho(\mathbf{R}',t'), \tag{6}$$

we may express the total induced electrostatic (self-) energy of the assembly of N particles as[57]

$$U_{\text{ind}} = \frac{1}{2} \int d^3\mathbf{R} \, \rho(\mathbf{R},t)\Phi_{\text{ind}}(\mathbf{R},t)$$

$$= \frac{1}{2} \int dz \int dz' \int \frac{d^2\mathbf{q}}{(2\pi)^2} \widetilde{G}_{\text{ind}}(\mathbf{q},z,z'; \mathbf{q}\cdot\mathbf{v})\widetilde{\rho}_0^*(\mathbf{q},z)\widetilde{\rho}_0(\mathbf{q},z')$$

$$= \frac{1}{2} \int \frac{d^2\mathbf{q}}{(2\pi)^2} \frac{2\pi}{q} |\mathcal{F}(\mathbf{q})|^2 \, \text{Re}\left[\frac{1}{\epsilon(q, \mathbf{q}\cdot\mathbf{v})} - 1\right], \tag{7}$$

where $\widetilde{\rho}_0(\mathbf{q},z)$ is a two-dimensional (2D) FT of the charge density in Eq. (5), while the form factor of the assembly is

defined by

$$\mathcal{F}(\mathbf{q}) = \sum_{j=1}^{N} \mathcal{Q}_j(\mathbf{q})e^{-i\mathbf{q}\cdot\mathbf{r}_j - qz_j}, \tag{8}$$

with $\mathcal{Q}_j(\mathbf{q}) = Z_j e - q\mu_j^{\perp} - i\,\mathbf{q}\cdot\boldsymbol{\mu}_j^{\parallel}$ being the charge form factor of the jth particle having the dipole components $\mu_j^{\perp}$ and $\boldsymbol{\mu}_j^{\parallel}$ that are perpendicular and parallel to graphene, respectively. In a similar manner, one may also define the rate of energy loss of the assembly of N particles by[70]

$$\frac{d\mathcal{E}}{dt} = -\int d^3\mathbf{R} \, \rho(\mathbf{R},t) \frac{\partial}{\partial t}\Phi_{\text{ind}}(\mathbf{r},z,t)$$

$$= -\int \frac{d^2\mathbf{q}}{(2\pi)^2} \frac{2\pi}{q} |\mathcal{F}(\mathbf{q})|^2 \, \mathbf{q}\cdot\mathbf{v} \, \text{Im}\left[\frac{1}{\epsilon(q, \mathbf{q}\cdot\mathbf{v})}\right]. \tag{9}$$

In the final expressions of Eqs. (7) and (9), we have used the symmetry of the dielectric function $\epsilon^*(q,\omega) = \epsilon(q,-\omega)$.

It is often of interest to assume that all particles have the same charges and dipole moments, so that $\mathcal{Q}_j(\mathbf{q}) \equiv \mathcal{Q}(\mathbf{q})$ for all j, allowing one to write $|\mathcal{F}(\mathbf{q})|^2 = |\mathcal{Q}(\mathbf{q})|^2 S(\mathbf{q})$, where the geometric effect of correlated charges is exposed via the structure factor

$$S(\mathbf{q}) = \sum_{j=1}^{N} e^{-2qz_j} + \sum_{j=1}^{N} \sum_{j\neq\ell=1}^{N} e^{i\mathbf{q}\cdot(\mathbf{r}_\ell - \mathbf{r}_j)}e^{-q(z_j + z_\ell)}. \tag{10}$$

Note that the first summation in this structure factor, when used in Eq. (7), represents independent contributions due to the self-energy, or the image potential of each particle or, when used in Eq. (9), it represents independent contributions due to the stopping force on each particle. On the other hand, the second term in Eq. (10) with double summation over the distinct particle pairs, when used in Eq. (7), represents contributions due to the dynamically screened pairwise interaction energies or, when used in Eq. (9), the double summation gives rise to the so-called vicinage, or the interference effect in the total energy loss of the assembly due to the spatial correlation among particles.[57]

While the above formalism may be readily used to study the interaction of graphene with an assembly of particles having arbitrary geometric configuration, we limit our focus to a few important special cases: a point dipole, two point ions with finite separation, and two static point dipoles with finite separation between them.

A. Point dipole

A point dipole with zero net charge may be regarded as a limit of two extremely correlated point charges of the opposite signs, having a vanishingly short relative position vector between them, $\mathbf{d} \rightarrow \mathbf{0}$, such that $Ze\mathbf{d} \rightarrow \boldsymbol{\mu} = \{\boldsymbol{\mu}_{\parallel}, \mu_z\}$ with $\boldsymbol{\mu}_{\parallel} = \{\mu_x, \mu_y\}$. One may evaluate the self-energy and the forces acting on a dipole grazingly scattered from graphene as follows.[63,64] With $\rho(\mathbf{R},t)$ in Eq. (6) replaced by the charge density $\rho_{\text{dip}}(\mathbf{R},t) = -\boldsymbol{\mu} \cdot \nabla_{\mathbf{R}} \delta[\mathbf{R} - \mathbf{R}_0(t)]$ that corresponds to a dipole moving parallel to graphene along the trajectory $\mathbf{R}_0(t) = \{\mathbf{v}t, z_0\}$ at a fixed distance z_0 above graphene, one

obtains the dipole self-energy as

$$U_{\text{dip}} = \frac{1}{2} \int d^3\mathbf{R}\, \rho_{\text{dip}}(\mathbf{R},t)\Phi_{\text{ind}}(\mathbf{R},t) = \frac{1}{2} \int_{-\infty}^{\infty} dt'\, (\boldsymbol{\mu}\cdot\nabla_{\mathbf{R}})(\boldsymbol{\mu}\cdot\nabla_{\mathbf{R}'})G_{\text{ind}}(\mathbf{R},\mathbf{R}';t-t')|_{\mathbf{R}=\mathbf{R}_0(t),\,\mathbf{R}'=\mathbf{R}_0(t')}$$

$$= \frac{1}{2} \int \frac{d^2\mathbf{q}}{(2\pi)^2} \frac{2\pi}{q}\big[(\mathbf{q}\cdot\boldsymbol{\mu}_{\|})^2 + q^2\mu_z^2\big]e^{-2qz_0}\,\text{Re}\!\left[\frac{1}{\epsilon(q,\mathbf{q}\cdot\mathbf{v})} - 1\right]. \tag{11}$$

With the induced electric field above graphene given by $\mathbf{E}_{\text{ind}}(\mathbf{R},t) = -\nabla_{\mathbf{R}}\Phi_{\text{ind}}(\mathbf{R},t)$, the total induced force on the dipole reads as

$$\mathbf{F}_{\text{ind}} = \int d^3\mathbf{R}\, \rho_{\text{dip}}(\mathbf{R},t)\mathbf{E}_{\text{ind}}(\mathbf{R},t) = -\int_{-\infty}^{\infty} dt'\, (\boldsymbol{\mu}\cdot\nabla_{\mathbf{R}})(\boldsymbol{\mu}\cdot\nabla_{\mathbf{R}'})\nabla_{\mathbf{R}}G_{\text{ind}}(\mathbf{R},\mathbf{R}';t-t')|_{\mathbf{R}=\mathbf{R}_0(t),\,\mathbf{R}'=\mathbf{R}_0(t')}$$

$$= -\int \frac{d^2\mathbf{q}}{(2\pi)^2} \frac{2\pi}{q}(i\mathbf{q} - q\hat{\mathbf{e}}_z)\big[(\mathbf{q}\cdot\boldsymbol{\mu}_{\|})^2 + q^2\mu_z^2\big]e^{-2qz_0}\left[\frac{1}{\epsilon(q,\mathbf{q}\cdot\mathbf{v})} - 1\right], \tag{12}$$

where $\hat{\mathbf{e}}_z$ is a unit vector in the direction of the z axis. Note that the rate of energy loss for a dipole, obtained from Eq. (9) with ρ replaced by ρ_{dip}, gives $(d\mathcal{E}/dt)_{\text{dip}} = -\mathbf{v}\cdot\mathbf{F}_{\text{ind}}$, showing that the component of the force [Eq. (12)] taken in the direction of motion is dissipative, giving rise to the stopping of the dipole due to the excitation of dynamic modes in graphene (and possibly the substrate, too). On the other hand, the force component from Eq. (12) that is perpendicular to graphene may be expressed in terms of the dipole self-energy [Eq. (11)] as $\hat{\mathbf{e}}_z\cdot\mathbf{F}_{\text{ind}} = -\partial U_{\text{dip}}/\partial z_0$, exposing its conservative nature that is related to the image interaction of the dipole with graphene (and the substrate).

If one assumes that the dipole moves with the velocity $\mathbf{v}$ that is directed along the x axis, then the total force on the dipole $\mathbf{F}_{\text{ind}} = \{F_x, F_y, F_z\}$ may be written as

$$F_x = -\frac{1}{z_0^4}\big[\mu_x^2 f_x^d + \mu_y^2 f_y^d + \mu_z^2(f_x^d + f_y^d)\big], \tag{13}$$

$$F_y = -\frac{2}{z_0^4}\mu_x\mu_y f_y^d, \tag{14}$$

$$F_z = -\frac{1}{z_0^4}\big[\mu_x^2 f_x^c + \mu_y^2 f_y^c + \mu_z^2(f_x^c + f_y^c)\big], \tag{15}$$

where the dissipative and conservative dimensionless force coefficients f_α^d and f_α^c are given, respectively, by

$$f_\alpha^d = -z_0^4 \int \frac{d^2\mathbf{q}}{2\pi} q_\alpha^2 \frac{q_x}{q} e^{-2qz_0}\,\text{Im}\!\left[\frac{1}{\epsilon(q,q_x v)}\right], \tag{16}$$

$$f_\alpha^c = -z_0^4 \int \frac{d^2\mathbf{q}}{2\pi} q_\alpha^2 e^{-2qz_0}\,\text{Re}\!\left[\frac{1}{\epsilon(q,q_x v)} - 1\right], \tag{17}$$

with $\alpha = x,y$. While the force components F_x and F_z are purely dissipative and purely conservative, respectively, and may be associated with the stopping force and the image force on the dipole, one notices that, somewhat surprisingly, there also exists a nonvanishing dissipative force F_y that is parallel to graphene but is perpendicular to the direction of motion, as long as the dipole components satisfy $\mu_x\mu_y \neq 0$.[63,64]

In order to study the effects of the dipole moment orientation, it may be useful to express its Cartesian components in terms of its magnitude $\mu = \|\boldsymbol{\mu}\|$ and the direction angles θ relative to the z axis and φ relative to the x axis (i.e., the direction of the dipole motion parallel to graphene), whence $\mu_x = \mu\sin\theta\cos\varphi$, $\mu_y = \mu\sin\theta\sin\varphi$, and $\mu_z = \mu\cos\theta$. Then, taking the angular average over all possible dipole orientations, one finds $\langle\mu_x^2\rangle = \langle\mu_y^2\rangle = \langle\mu_z^2\rangle = \mu^2/3$ and $\langle\mu_x\mu_y\rangle = 0$, so that the corresponding averaged force components are $\langle F_y\rangle = 0$, whereas $\langle F_x\rangle = (\mu^2/6)\partial^2 F_s^u/\partial z_0^2$ and $\langle F_z\rangle = (\mu^2/6)\partial^2 F_{\text{im}}^u/\partial z_0^2$ show clear and simple relations with the corresponding stopping and image forces F_s^u and F_{im}^u that act on a point ion with unit charge, given by, respectively,[33]

$$F_s^u = \frac{2}{\pi v} \int_0^\infty dq\, e^{-2qz_0} \int_0^{qv} d\omega\, \frac{\omega}{\sqrt{q^2v^2 - \omega^2}}\,\text{Im}\!\left[\frac{1}{\epsilon(q,\omega)}\right], \tag{18}$$

$$F_{\text{im}}^u = \frac{2}{\pi} \int_0^\infty dq\, q\, e^{-2qz_0} \int_0^{qv} \frac{d\omega}{\sqrt{q^2v^2 - \omega^2}}\,\text{Re}\!\left[\frac{1}{\epsilon(q,\omega)} - 1\right]. \tag{19}$$

Finally, the torque acting on the dipole about its center of mass in the moving frame of reference may be evaluated as[64]

$$\boldsymbol{\tau} = \int d^3\mathbf{R}\, \rho_{\text{dip}}(\mathbf{R},t)[\mathbf{R} - \mathbf{R}_0(t)]\times\mathbf{E}_{\text{ind}}(\mathbf{R},t) = -\int_{-\infty}^{\infty} dt'\, (\boldsymbol{\mu}\times\nabla_{\mathbf{R}})(\boldsymbol{\mu}\cdot\nabla_{\mathbf{R}'})G_{\text{ind}}(\mathbf{R},\mathbf{R}';t-t')|_{\mathbf{R}=\mathbf{R}_0(t),\,\mathbf{R}'=\mathbf{R}_0(t')}$$

$$= \int \frac{d^2\mathbf{q}}{(2\pi)^2} \frac{2\pi}{q}[\boldsymbol{\mu}\times(i\mathbf{q} - q\hat{\mathbf{e}}_z)][\boldsymbol{\mu}\cdot(i\mathbf{q} + q\hat{\mathbf{e}}_z)]e^{-2qz_0}\left[\frac{1}{\epsilon(q,\mathbf{q}\cdot\mathbf{v})} - 1\right]. \tag{20}$$

For a dipole moving with speed v along the x axis, the Cartesian components of the torque on the dipole $\boldsymbol{\tau} = \{\tau_x,\tau_y,\tau_z\}$ may be written as

$$\tau_x = -\frac{1}{z_0^3}\big(-\mu_y\mu_z m_x^c + \mu_x\mu_y m^d\big), \tag{21}$$

$$\tau_y = -\frac{1}{z_0^3}\left[\mu_x\mu_z m_y^c - (\mu_x^2 + \mu_z^2)m^d\right], \qquad (22)$$

$$\tau_z = -\frac{1}{z_0^3}\left[\mu_x\mu_y(m_x^c - m_y^c) + \mu_y\mu_z m^d\right], \qquad (23)$$

where the dissipative and conservative dimensionless torque coefficients m^d and m_α^c are given, respectively, by

$$m^d = -z_0^3 \int \frac{d^2\mathbf{q}}{2\pi} q_x e^{-2qz_0} \operatorname{Im}\left[\frac{1}{\epsilon(q, q_x v)}\right], \qquad (24)$$

$$m_\alpha^c = -z_0^3 \int \frac{d^2\mathbf{q}}{2\pi} \frac{q_\alpha^2}{q} e^{-2qz_0} \operatorname{Re}\left[\frac{1}{\epsilon(q, q_x v)} - 1\right], \qquad (25)$$

with $\alpha = x, y$. One notices that all three components of the torque generally consist of both the dissipative and conservative contributions. In the case of a randomly oriented dipole, one finds that $\langle\tau_x\rangle = \langle\tau_z\rangle = 0$, whereas the only nonvanishing component $\langle\tau_y\rangle = (\mu^2/3)\partial F_s^u/\partial z_0 > 0$ is clearly dissipative and amounts to the dipole "rolling" along the surface of graphene as it moves at the speed v.

B. Separated particles

The case of two ions at finite separation that have equal charges Ze and zero dipole moments is of interest, e.g., for analyzing the electrostatic interaction energy in the coadsorption of alkali-metal atoms on a surface,[6–8,15,16] or for studying the comoving ion fragments during Coulomb explosion of a homonuclear diatomic molecule on a surface.[56,57,60,61] In the latter case, experiments and simulations of grazing scattering of molecules from surfaces showed that the internuclear axis tends to remain parallel to the surface during Coulomb explosion.[55–62] In either case, it is then worthwhile studying the configuration of two point ions at equal and fixed distances z_0 from graphene with their relative position vector $\mathbf{d} = \mathbf{r}_2 - \mathbf{r}_1$ parallel to the graphene, giving a simple structure factor of the form

$$S(\mathbf{q}) = 2e^{-2qz_0}[1 + \cos(\mathbf{q} \cdot \mathbf{d})]. \qquad (26)$$

If one uses the second term from this expression in Eq. (7) and combines it with the bare Coulomb interaction for two ions a distance $d = \|\mathbf{r}_2 - \mathbf{r}_1\|$ apart, one obtains the total screened interaction energy between the ions as

$$U_{\text{scr}}^i = \frac{Z^2 e^2}{d} + \frac{Z^2 e^2}{2\pi} \int \frac{d^2\mathbf{q}}{q} e^{-2qz_0} \cos(\mathbf{q} \cdot \mathbf{d})$$
$$\times \operatorname{Re}\left[\frac{1}{\epsilon(q, \mathbf{q} \cdot \mathbf{v})} - 1\right]. \qquad (27)$$

On the other hand, by using the full structure factor from Eq. (26) in Eq. (9), one may write the total energy loss of two ions as the sum $(d\mathcal{E}/dt)_{\text{tot}} = 2(d\mathcal{E}/dt)_{\text{ion}} + (d\mathcal{E}/dt)_{\text{vic}}$, where $(d\mathcal{E}/dt)_{\text{ion}} = -vZ^2 e^2 F_s^u > 0$ is the loss rate for a single independent ion of charge Ze [see Eq. (18)], while

$$\left(\frac{d\mathcal{E}}{dt}\right)_{\text{vic}} = -\frac{Z^2 e^2}{\pi} \int \frac{d^2\mathbf{q}}{q} e^{-2qz_0} \cos(\mathbf{q} \cdot \mathbf{d}) \, \mathbf{q} \cdot \mathbf{v}$$
$$\times \operatorname{Im}\left[\frac{1}{\epsilon(q, \mathbf{q} \cdot \mathbf{v})}\right] \qquad (28)$$

describes the vicinage effect in the energy loss. It is customary to analyze the vicinage effect in terms of the ratio

$R = (d\mathcal{E}/dt)_{\text{vic}}/[2(d\mathcal{E}/dt)_{\text{ion}}]$ for various orientations of the interionic axis $\mathbf{d}$ with respect to the velocity vector $\mathbf{v}$.[57] Two special cases are of particular interest. Namely, when $\mathbf{d}$ is directed along $\mathbf{v}$ one expects strong destructive interference effects in the energy loss, whereas randomly oriented interionic axis is of interest for statistical analysis of Coulomb explosions on surfaces. In the latter case, one may perform 2D averaging over the orientation angles of $\mathbf{d}$, which amounts to replacing the factor $\cos(\mathbf{q} \cdot \mathbf{d})$ in Eqs. (27) and (28) by $\langle\cos(\mathbf{q} \cdot \mathbf{d})\rangle = J_0(qd)$, where J_0 is the Bessel function of zeroth order. Then, the resulting ratio R_{rand} has two obvious limits as a function of distance d, i.e., $R_{\text{rand}} \to 1$ when $d \to 0$ and $R_{\text{rand}} \to 0$ when $d \to \infty$.

Finally, it is interesting to consider a system of static ($\mathbf{v} = \mathbf{0}$) point dipoles with zero charge, which are placed at the positions $\mathbf{R}_j = \{\mathbf{r}_j, z_j\}$ and have the dipole moments $\boldsymbol{\mu}_j$, the orientations of which may vary from dipole to dipole. The total induced self-energy of this system may be written as

$$U_{\text{ind}}^d = \sum_{j=1}^N U_{\text{dip}}^{(j)} + \frac{1}{2}\sum_{j=1}^N \sum_{j \neq \ell=1}^N (\boldsymbol{\mu}_j \cdot \nabla_{\mathbf{R}_j})(\boldsymbol{\mu}_\ell \cdot \nabla_{\mathbf{R}_\ell})$$
$$\times \int_0^\infty dq \, e^{-q(z_j + z_\ell)} J_0(qr_{j\ell})\left[\frac{1}{\epsilon(q)} - 1\right], \qquad (29)$$

where $U_{\text{dip}}^{(j)}$ is the individual self-energy of the jth dipole defined in Eq. (11) with $\mathbf{v} = \mathbf{0}$, $r_{j\ell} = \|\mathbf{r}_\ell - \mathbf{r}_j\|$ is the projected interdipole distance in the plane of graphene, and $\epsilon(q)$ is the static dielectric function of the system. The second term in Eq. (29) with double summation is responsible for a graphene- (and substrate-) mediated interaction between the dipoles. For a special case of two dipoles with the moments $\boldsymbol{\mu}_1$ and $\boldsymbol{\mu}_2$ that are placed at equal distances z_0 above graphene with their relative position vector $\mathbf{d} = \mathbf{r}_2 - \mathbf{r}_1$ being parallel to graphene, the second term in Eq. (29) gives

$$U_{\text{int}}^d = \mu_1^\perp \mu_2^\perp V_0 + [\mu_1^\perp(\boldsymbol{\mu}_2^\parallel \cdot \hat{\mathbf{d}}) + \mu_2^\perp(\boldsymbol{\mu}_1^\parallel \cdot \hat{\mathbf{d}})]V_1$$
$$+ \frac{1}{2}\boldsymbol{\mu}_1^\parallel \cdot \boldsymbol{\mu}_2^\parallel(V_0 + V_2) - (\boldsymbol{\mu}_1^\parallel \cdot \hat{\mathbf{d}})(\boldsymbol{\mu}_2^\parallel \cdot \hat{\mathbf{d}})V_2, \qquad (30)$$

where $\hat{\mathbf{d}} = \mathbf{d}/d$ is a unit vector in the direction of the interdipolar axis, and the coefficients V_k are given for $k = 0, 1,$ and 2 by

$$V_k = \int_0^\infty dq \, q^2 e^{-2qz_0} J_k(qd)\left[\frac{1}{\epsilon(q)} - 1\right], \qquad (31)$$

with J_k being a Bessel function of order k. With the bare Coulombic interaction between two point dipoles being written for the present configuration as

$$U_C^d = \frac{1}{d^3}[\mu_1^\perp \mu_2^\perp + \boldsymbol{\mu}_1^\parallel \cdot \boldsymbol{\mu}_2^\parallel - 3(\boldsymbol{\mu}_1^\parallel \cdot \hat{\mathbf{d}})(\boldsymbol{\mu}_2^\parallel \cdot \hat{\mathbf{d}})], \qquad (32)$$

the total screened dipole-dipole interaction energy on graphene is obtained from Eqs. (30) and (32) as $U_{\text{scr}}^d = U_C^d + U_{\text{int}}^d$.

III. RESULTS AND DISCUSSION

In this section, we first provide a discussion of the interaction of a moving point dipole with graphene, which is followed by a discussion of several results for two separated ions and two separated dipoles. The polarization function $\Pi(q, \omega)$ of doped graphene with finite charge carrier density n

describes three types of excitations in graphene's π-electron bands that may be characterized by different regions in the first quadrant of the (q,ω) plane.[18,30–33] The interband SPEs occur in the region $\omega/v_F > \max(q, 2k_F - q)$, while the intraband SPEs occur in the region $q > \omega/v_F > \max(q - 2k_F, 0)$, where $k_F = \sqrt{\pi n}$ is graphene's Fermi wave number (we assume $n > 0$ without loss of generality). In addition, a well-defined plasmon mode exists in the region $q < \omega/v_F < 2k_F - q$ for $q < k_F$ that exhibits a $\omega \propto \sqrt{q}$ dispersion relation at long wavelengths.

In the case of intrinsic graphene ($n = 0$), the polarization function has a particularly simple form, given by[18,30–33]

$$\Pi_0(q,\omega) = \frac{q^2}{4\hbar}\left[\frac{\mathcal{U}(qv_F - \omega)}{\sqrt{(qv_F)^2 - \omega^2}} + i\frac{\mathcal{U}(\omega - qv_F)}{\sqrt{\omega^2 - (qv_F)^2}}\right], \quad (33)$$

where $\mathcal{U}$ is the Heaviside unit step function, which reflects the fact that only the interband SPEs are allowed in the region $\omega > v_F q$. As a consequence, for intrinsic graphene supported by a substrate with zero gap ($h = 0$) and with static dielectric constant ϵ_{sub}, so that $\epsilon_{bg} = \epsilon_{bg}^0 \equiv (\epsilon_{sub} + 1)/2$, the resulting dielectric function of the system $\epsilon(q,\omega)$ only depends on the ratio ω/q, so that the dependence of various quantities on spatial variables, such as the distance z_0 and the separation d, may be factored out. For example, one finds from Eqs. (18) and (19) that both the stopping and image forces on a point ion with the charge Ze are proportional to the factor $F_0^i = Z^2 e^2/z_0^2$ that is multiplied by certain universal functions of the reduced ion speed v/v_F, the coupling constant of free graphene $r_s = e^2/(\hbar v_F) \approx 2.19$, and the background dielectric constant ϵ_{bg}^0.[33] Similarly, from Eqs. (12) and (20), one may easily find that, for intrinsic graphene, the force components and the torque components on a point dipole with the moment μ are proportional to the factors $F_0^d = \mu^2/z_0^4$ and $\tau_0 = \mu^2/z_0^3$, respectively [hence the factorizations in Eqs. (13)–(15) and (21)–(23)].

Regarding the parameter space, the default model for graphene is free graphene with zero damping, but we briefly discuss the effects of polarizable substrate and finite damping in graphene's dielectric response, as well as the effects of replacing graphene with m2DEG. As for the particles that interact with graphene, for a moving dipole we are mostly concerned with the dependence of the results on its velocity, while for the separated particles we are mostly concerned with the dependence of the results on the interparticle separation d.

A. Moving point dipole

Since the line $\omega = v_F q$ represents a boundary that separates the regions in the first quadrant of the (q,ω) plane where interband and intraband SPEs take place, whereas the kinematic constraints imply a resonance condition in the form $\omega = vq$ for excitation of such modes by an external particle that moves at speed v parallel to graphene, it is natural to represent the velocity dependence of various quantities in terms of the normalized speed v/v_F. Comparison with previous results[64] may be facilitated by noting that the Fermi speed for graphene's π-electron bands is given by $v_F \approx 0.46$ atomic units.
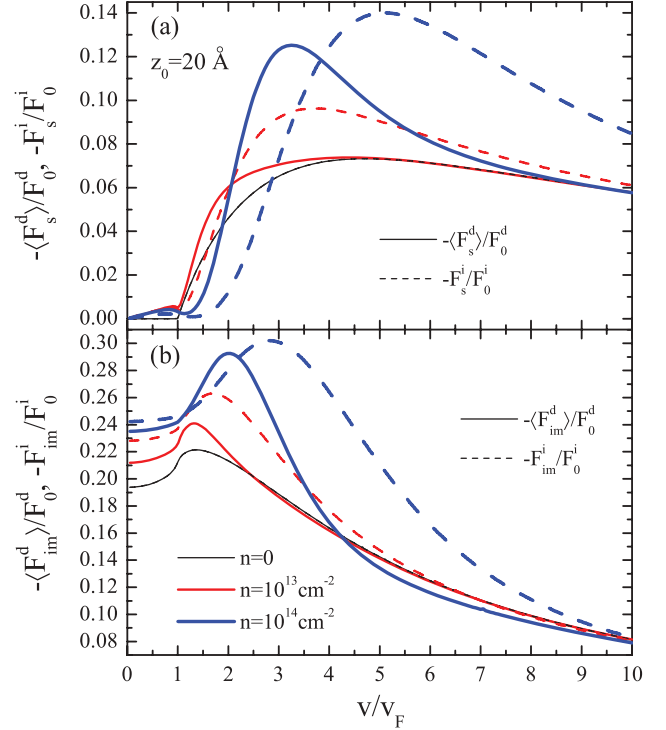
FIG. 1. (Color online) Stopping force $\langle F_s^d \rangle$ (a) and image force $\langle F_{im}^d \rangle$ (b) on a randomly oriented point dipole (solid lines), normalized by $F_0^d = \mu^2/z_0^4$, and the stopping force F_s^i (a) and image force F_{im}^i (b) on a point ion (dashed lines), normalized by $F_0^i = Z^2 e^2/z_0^2$, both moving at distance $z_0 = 20$ Å above free graphene, are shown as functions of the reduced speed v/v_F for graphene doping densities: $n = 0$ (thin black solid lines coincide with thin black dashed lines), $n = 10^{13}$ cm^{-2} [medium gray (red) lines], and $n = 10^{14}$ cm^{-2} [thick gray (blue) lines].

1. Comparison with point ion

We first compare the stopping and image forces on a randomly oriented point dipole $\langle F_s^d \rangle \equiv \langle F_x \rangle$ and $\langle F_{im}^d \rangle \equiv \langle F_z \rangle$, with the corresponding forces on a point ion, obtained from Eqs. (18) and (19) as $F_s^i \equiv Z^2 e^2 F_s^u$ and $F_{im}^i \equiv Z^2 e^2 F_{im}^u$. In Fig. 1, we show the projectile velocity dependencies of those forces, normalized by the factors $F_0^d = \mu^2/z_0^4$ and $F_0^i = Z^2 e^2/z_0^2$ for the dipole and the ion, respectively, for several doping densities of free graphene ($\epsilon_{sub} = 1$ or $h \to \infty$). With such a normalization, the cases of a dipole and an ion above intrinsic graphene ($n = 0$) give identical curves (shown by the thin black lines in Fig. 1), emphasizing the universality of their scaling by the respective factors F_0^d and F_0^i. Note that the shapes of those curves for intrinsic graphene are determined essentially by the interband SPEs and, as a consequence, both stopping forces vanish for projectile speeds $v < v_F$.[33] This universality of scaling is lost for finite charge carrier density n because the polarization function of doped graphene $\Pi(q,\omega)$ no longer depends on the ratio ω/q alone, as in the case of intrinsic graphene, but rather introduces a new length scale given by the inverse Fermi wave number k_F^{-1}, which differently affects the results for ion and dipole. We have found that, with increasing charge carrier density in graphene n, there is very little change in both forces on the dipole, as compared to the

change found in the forces on the ion, especially at densities $n \lesssim 10^{11}$ cm^{-2}. For that reason, we only show in Fig. 1 cases with two rather large doping densities of graphene, in addition to the case $n = 0$.

In order to further pursue the comparison with an ion, we also evaluate the induced charge carrier densities in free graphene n_{ind} due to a point dipole and due to a point ion moving parallel to graphene at a distance $z_0 > 0$. It was shown in Ref. 35 that the induced density in graphene due to the point ion moving at speeds $v > v_F$ exhibits strong wake patterns, and we wish to examine how the direction of the dipole moment affects such a wake for a moving dipole. Using the results from the Appendix, we show in Fig. 2 the normalized densities $n_{\text{ind}}^{\text{i}} z_0^2$ for an ion, and $n_{\text{ind}}^{\text{d}} z_0^3 e/\mu$ for a dipole with

the orientation angles $\theta = 90°$ and $\varphi = 90°$ (i.e., the dipole moment being parallel to graphene and perpendicular to the direction of motion), both moving with the speed of $v = 4v_F$ at the distance $z_0 = 20$ Å from free graphene with equilibrium charge carrier density $n = 10^{13}$ cm^{-2}. One notices that the two particles induce similar, V-shaped wake patterns in the graphene plane that trail the projection of each particle, with an important difference that the pattern due to the dipole is asymmetric about the x axis (the direction of motion), while the pattern due to the ion is symmetric. While this difference between the surface wakes induced by a moving ion and a moving dipole is not an exclusive property of graphene, it seems that experimental verification of such a difference is still pending.

2. Forces and torque on moving dipole

The asymmetry of the wake pattern in the induced charge density in free graphene implies that the effects of dipole orientation may be strong. Equations (13)–(15) and (21)–(23) show that the Cartesian components of the forces and the torque acting on a dipole moving at speed v along the x axis with arbitrary orientation of its dipole moment may be expressed in terms of several coefficients f_α^{d} and f_α^{c} defined in Eqs. (16) and (17), as well as m^{d} and m_α^{c} defined in Eqs. (24) and (25), which clearly expose dissipative and conservative contributions. Note that these coefficients are rendered in dimensionless form, in conjunction with the scaling factors z_0^{-4} and z_0^{-3} that are introduced in Eqs. (13)–(15) and (21)–(23), respectively, and with their signs chosen so that the dissipative coefficients are always positive, while positive values of the conservative force coefficients correspond to attraction towards graphene.

In Fig. 3, we show those coefficients for a free, intrinsic graphene ($n = 0$), when the coefficients are actually independent of z_0 and are universal functions of v/v_F. One notices resonant features in all coefficients at the dipole speeds $v \lesssim 3v_F$, similar to those observed in Fig. 1, which result from the onset of the interband SPEs in intrinsic graphene. We further examine the effects of finite doping with $n = 10^{13}$ cm^{-2} and finite damping with the damping constant $\hbar\gamma = 400$ meV, which is treated by using a Mermin modified polarization function for graphene.[33,71] One notices in Fig. 3 that both n and γ have similar effects on the coefficients in softening their resonant features. This is especially obvious for the dissipative coefficients for $v < v_F$, which seem to acquire a linear increase with v at low speeds, with a rate that is proportional to both n and γ, in a similar manner as was found for point ions.[33] As pointed out in Ref. 34, linear dependence of dissipative forces on velocity is relevant to the friction phenomena on surfaces,[65–67] so that the results from Fig. 3 imply that friction of slow dipoles on graphene may be efficiently controlled by its doping density n.

In Fig. 4, we examine the effects of different distances z_0 and of graphene doping at the densities $n = 10^{13}$ cm^{-2} and 10^{14} cm^{-2} over a broader range of dipole speeds. While the latter density may be unrealistically high for graphene, we use it, here and elsewhere, to examine the regime where the role of interband SPEs is expected to be suppressed with respect to the roles of intraband SPEs and plasmon excitations, thereby
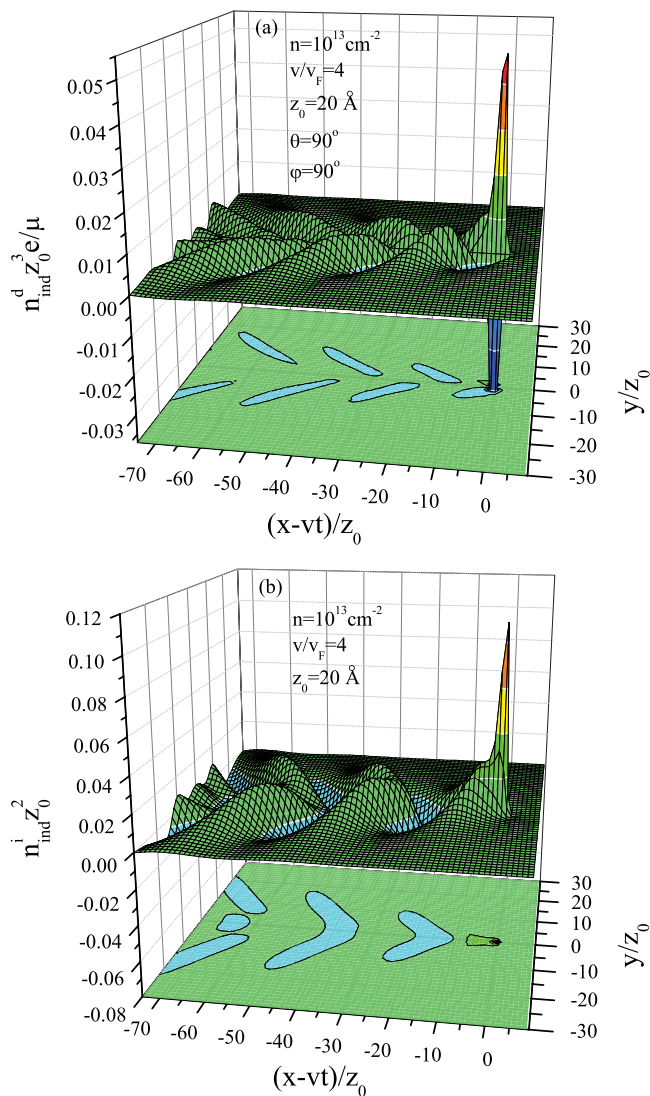
FIG. 2. (Color online) Induced charge densities in free graphene with doping density of $n = 10^{13}$ cm^{-2} are shown as functions of the normalized coordinates $\{x - vt, y\}$ in a moving frame by using the reduced units: $n_{\text{ind}}^{\text{d}} z_0^3 e/\mu$ for a point dipole (a) with a dipole moment $\boldsymbol{\mu}$ oriented along the y axis (i.e., parallel to graphene and perpendicular to the direction of motion), and $n_{\text{ind}}^{\text{i}} z_0^2$ for a point ion (b) of charge Ze, both moving with the speed of $v = 4v_F$ in the direction of the x axis, at a fixed distance $z_0 = 20$ Å from graphene.
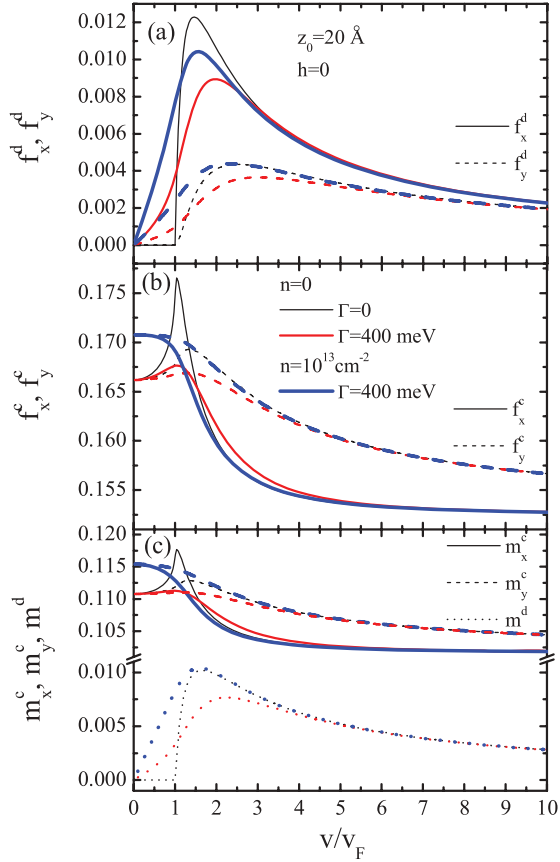
FIG. 3. (Color online) Panel (a) shows dissipative coefficients f_x^d (solid lines) and f_y^d (dashed lines), and panel (b) shows conservative coefficients f_x^c (solid lines) and f_y^c (dashed lines) from Eqs. (13)–(15) for the force components on a point dipole, whereas panel (c) shows conservative coefficients m_x^c (solid lines) and m_y^c (dashed lines), and the dissipative coefficient m^d (dotted lines) from Eqs. (21)–(23) for the torque components on a point dipole, as functions of the reduced speed v/v_F of the dipole moving at the distance $z_0 = 20$ Å above free graphene for three combinations of the doping density n and the damping constant $\Gamma \equiv \hbar\gamma$ with $n = 0$ and $\Gamma = 0$ (thin black lines), $n = 0$ and $\Gamma = 400$ meV [medium gray (red) lines], and $n = 10^{13}$ cm^{-2} and $\Gamma = 400$ meV [thick gray (blue) lines].

making graphene more akin to a m2DEG with single parabolic band energy.[2] One notices in Fig. 4 that increasing both n and z_0 may exert strong influence on various coefficients (within the adopted normalization), and may even give rise to a change of sign in the conservative coefficients f_x^c and m_x^c, which could then result in the change of sign in the resulting forces and/or torques in Eqs. (13)–(15) and (21)–(23). A similar effect was observed for a dipole moving over m2DEG described by a two-fluid, 2D hydrodynamic model, where the image force on the dipole was found to become repulsive for certain ranges of the speed and the dipole orientations.[64]

Given the importance of the m2DEG model in various studies of particle interactions with metallic surface state bands,[7–9,19,38–40] it is worthwhile comparing the dipole force and torque coefficients for free graphene with those for free m2DEG within the RPA.[68] This is performed in Fig. 5 for the electron density $n = 10^{13}$ cm^{-2} in both systems, and with the effective mass of the m2DEG chosen to be $m_{\text{eff}} = \hbar k_F/v_F$,

ensuring that both graphene and the m2DEG have the same plasmon dispersion relation at small wave numbers q. This criterion for choosing m_{eff} is adopted because high-velocity features in the stopping and image forces on a point ion moving over m2DEG are dominated by the plasmon excitations in that system.[68] One notices in Fig. 5 generally similar resonant features in the coefficients for both systems at lower speeds, say, $v \lesssim 5v_F$, but marked differences are seen at higher speeds, where both the dissipative and conservative coefficients seem to be more abundant and to decay slower with increasing speed for graphene than for m2DEG. Similar observations were made for point ions, where an explanation was provided in terms of the prevailing role of the interband SPEs in graphene, even in the regime of heavy doping.[40] It is interesting that, in comparison with the results shown in Fig. 4, one observes in Fig. 5 that the conservative coefficients f_x^c and m_x^c for the m2DEG may also change their signs, albeit at lower speeds and at lower density than in the case of graphene [see Figs. 4(d) and 4(f)].

Finally, the effects of substrate are also expected to be important for interactions with external particles, not only due to variations in the gap size h,[33,34] but also in the case when a substrate supports surface phonons.[34,37] For example, for an epitaxial graphene grown on a SiC substrate, which is characterized by a nondispersing transverse optical (TO) phonon mode with frequency $\hbar\omega_{\text{TO}} \approx 97$ meV and damping rate $\hbar\gamma_{\text{TO}} \approx 10$ meV, one may use a dielectric function of the form[72,73]

$$\epsilon_{\text{sub}}(\omega) = \epsilon_\infty + (\epsilon_0 - \epsilon_\infty)\frac{\omega_{\text{TO}}^2}{\omega_{\text{TO}}^2 - \omega(\omega + i\gamma_{\text{TO}})}, \quad (34)$$

where $\epsilon_\infty = \lim_{\omega\to\infty} \epsilon_{\text{sub}}(\omega) \approx 6.5$ and $\epsilon_0 = \epsilon_{\text{sub}}(0) \approx 9.7$ are the high-frequency and the static dielectric constants of SiC, respectively.[72,73] In Fig. 6, we analyze the force and the torque coefficients for a dipole moving over graphene with the charge carrier density $n = 10^{13}$ cm^{-2}, supported by a SiC substrate with zero gap that is described by either the full dielectric function in Eq. (34), or by its static limit ϵ_0. Also shown in Fig. 6 are the results for the case of no graphene, that is, for a point dipole moving over a SiC surface that supports a TO phonon mode. As expected, resonant features due to excitations of the substrate phonon are qualitatively most distinct at the lowest dipole speeds $v < v_F$, but the presence of the substrate phonon also affects the magnitude of all coefficients at high speeds by a surprisingly large amount. Similar effects were observed for a point ion moving over graphene epitaxially grown on a SiC substrate.[34,37]

B. Separated particles

As already mentioned in Sec. II B, in the case of two particles we are interested in the electrostatic part of the interparticle interaction energy due to screening by graphene, which depends on the interparticle separation d, while leaving out particles' individual self-energies because they do not depend on d and they only shift the overall energy reference level as a function of the distance from graphene. In the case of coadsorbed particles, we note that their interaction may be substantially affected at short separations by a direct chemical bond between the particles, as well as by their hybridization
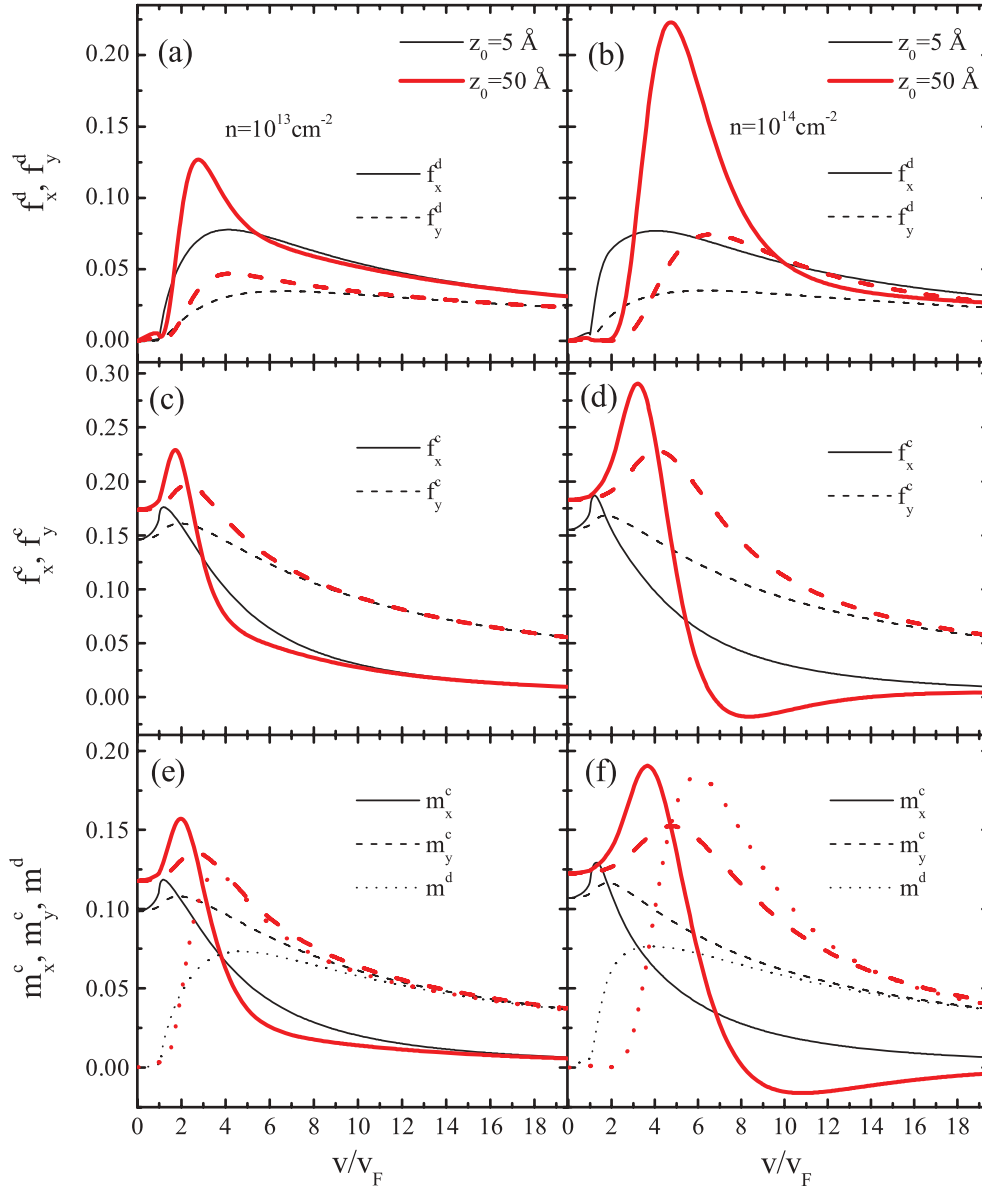
FIG. 4. (Color online) Panels (a) and (b) show dissipative coefficients f_x^d (solid lines) and f_y^d (dashed lines), and panels (c) and (d) show conservative coefficients f_x^c (solid lines) and f_y^c (dashed lines) from Eqs. (13)–(15) for the force components on a point dipole, whereas panels (e) and (f) show conservative coefficients m_x^c (solid lines) and m_y^c (dashed lines), and the dissipative coefficient m^d (dotted lines) from Eqs. (21)–(23) for the torque components on a point dipole, as functions of the reduced speed v/v_F of the dipole moving at two distances: $z_0 = 5$ Å (thin black lines) and $z_0 = 50$ Å [thick gray (red) lines] above free graphene with two doping densities: $n = 10^{13}$ cm^{-2} [panels (a), (c), (e)] and $n = 10^{14}$ cm^{-2} [panels (b), (d), (f)], and zero damping.

with graphene. In order to be able to discard such atomistic effects in the interacting system, we assume d to exceed a critical distance d_c on the order of the chemical bond length between the particles, and we limit our considerations to either the closed-shell atoms/molecules or particles that do not hybridize with graphene's π orbitals.[10,12]

In order to emphasize the effects of charge carrier density in doped graphene on the interparticle interaction energy, we note that the screening due to polarization of graphene is governed by its Thomas-Fermi (TF) wave number, given by $q_{TF} = 4r_s k_F$. Hence, we adopt a normalization of the interparticle separation by the inverse Fermi wave number

$k_F d$, and we accordingly normalize the interaction energies by $U_0^i = Z^2 e^2 k_F$ for ions and $U_0^d = \mu^2 k_F^3$ for dipoles. While such normalization allows us to show results that cover a broad range of charge carrier densities in doped graphene, it prevents us from making direct comparison with intrinsic graphene because $k_F = 0$ in that case. Such a comparison may be accomplished by adopting a normalization of the interparticle separation by the separation of each particle from its image in the plane of graphene $d/(2z_0)$, while normalizing the interaction energies between two ions and between two dipoles by the corresponding bare Coulombic interaction energies $U_C^i = Z^2 e^2/d$ and $U_C^d = \mu^2/d^3$.
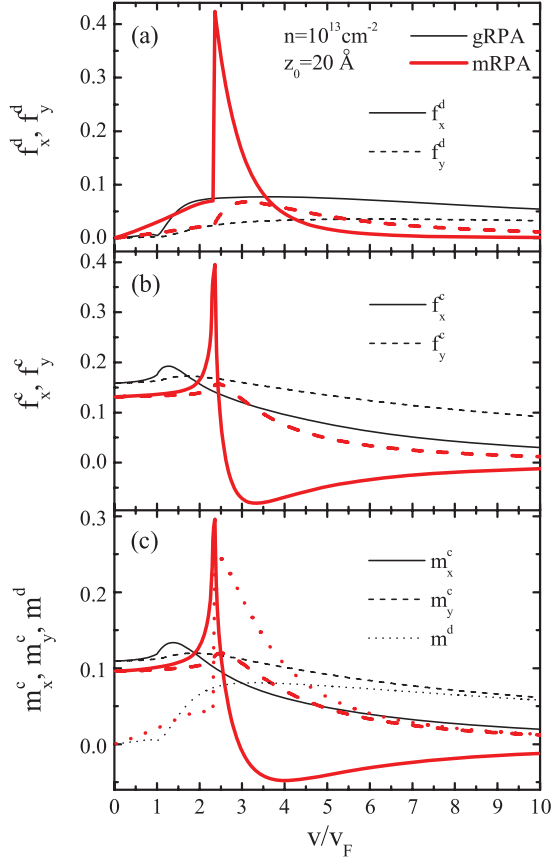
FIG. 5. (Color online) Panel (a) shows dissipative coefficients f_x^{d} (solid lines) and f_y^{d} (dashed lines), and panel (b) shows conservative coefficients f_x^{c} (solid lines) and f_y^{c} (dashed lines) from Eqs. (13)–(15) for the force components on a point dipole, whereas panel (c) shows conservative coefficients m_x^{c} (solid lines) and m_y^{c} (dashed lines), and the dissipative coefficient m^{d} (dotted lines) from Eqs. (21)–(23) for the torque components on a point dipole, as functions of the reduced speed v/v_F of the dipole moving at the distance $z_0 = 20$ Å above free graphene with doping density $n = 10^{13}$ cm^{-2} (thin black lines), and above free massive 2DEG with electron density $n = 10^{13}$ cm^{-2} [thick gray (red) lines].

1. Two static ions

We first consider a pair of static ions with equal charges Ze at equal distances z_0 from a free, doped graphene. Results are shown in Fig. 7 for the total screened interaction energy $U_{\mathrm{scr}}^{\mathrm{i}}$ from Eq. (27) with $\mathbf{v} = \mathbf{0}$, normalized by $U_0^{\mathrm{i}} = Z^2 e^2 k_F$, as a function of the reduced interionic separation $k_F d$ for several distances z_0 and for several doping densities n. One notices that the thus normalized interaction energy between the ions has the shortest range at the lowest density $n = 10^{11}$ cm^{-2}, which is least affected by increasing z_0. By a comparison with the bare Coulomb interaction $U_{\mathrm{C}}^{\mathrm{i}} = Z^2 e^2/d$, also shown in Fig. 7 (by the dashed lines), one notices that doped graphene provides substantial screening at all densities n. Moreover, the insets in Fig. 7 show shallow minima in the interaction energy due to FOs, which are most pronounced at lower densities n and shorter distances z_0. These oscillations may be discussed by rewriting the total screened interaction energy from Eq. (27)
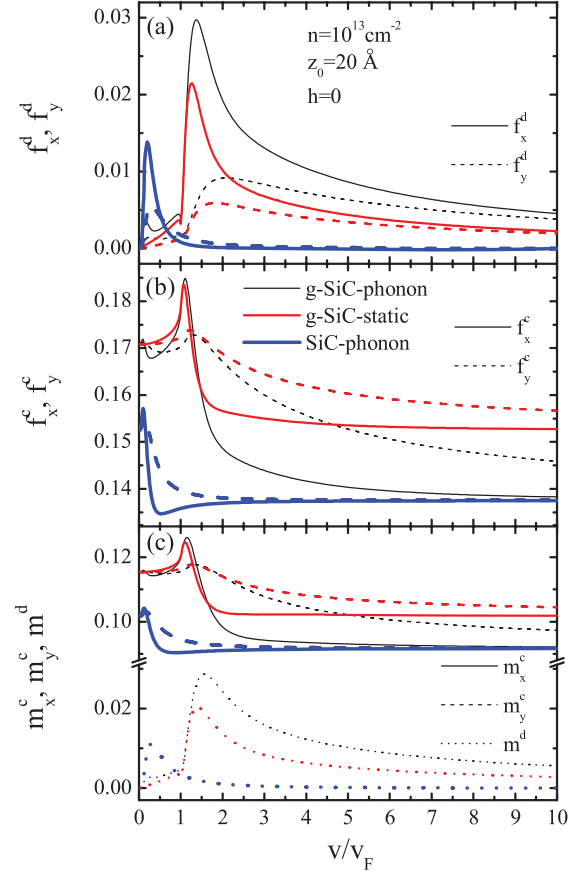
FIG. 6. (Color online) Panel (a) shows dissipative coefficients f_x^{d} (solid lines) and f_y^{d} (dashed lines), and panel (b) shows conservative coefficients f_x^{c} (solid lines) and f_y^{c} (dashed lines) from Eqs. (13)–(15) for the force components on a point dipole, whereas panel (c) shows conservative coefficients m_x^{c} (solid lines) and m_y^{c} (dashed lines), and the dissipative coefficient m^{d} (dotted lines) from Eqs. (21)–(23) for the torque components on a point dipole, as functions of the reduced speed v/v_F of the dipole moving at the distance $z_0 = 20$ Å above: graphene with doping density $n = 10^{13}$ cm^{-2} on a SiC substrate that supports a surface phonon (thin black lines), graphene with doping density $n = 10^{13}$ cm^{-2} on a SiC substrate described by a static dielectric constant [medium gray (red) lines], and SiC supporting a surface phonon with no graphene atop of it [thick gray (blue) lines]. The graphene-substrate gap is $h = 0$ in all cases.

as $U_{\mathrm{scr}}^{\mathrm{i}} = U_{\mathrm{TF}}^{\mathrm{i}} + U_{\mathrm{FO}}^{\mathrm{i}}$, where

$$U_{\mathrm{TF}}^{\mathrm{i}} = \frac{Z^2 e^2}{d} + Z^2 e^2 \int_0^\infty dq \, e^{-2qz_0} \, J_0(qd) \left[\frac{1}{\epsilon_{\mathrm{TF}}(q)} - 1 \right] \tag{35}$$

is the interaction energy between the ions in a TF approximation with the corresponding approximate dielectric function $\epsilon_{\mathrm{TF}}(q) = 1 + q_{\mathrm{TF}}/q$, whereas $U_{\mathrm{FO}}^{\mathrm{i}}$ gives an oscillatory part of the interaction arising from a discontinuity of the full static RPA dielectric function at $q = 2k_F$.[17,18] While $U_{\mathrm{TF}}^{\mathrm{i}}$ describes a smooth repulsive interaction with an asymptotic form $U_{\mathrm{TF}}^{\mathrm{i}} \propto Z^2 e^2/(q_{\mathrm{TF}}^2 d^3)$ for $z_0 \ll q_{\mathrm{TF}}^{-1} \ll d$,[74] the asymptotic behavior of the oscillatory part goes as[2,18]

$$U_{\mathrm{FO}}^{\mathrm{i}} \propto \frac{Z^2 e^2 q_{\mathrm{TF}}}{(2k_F + q_{\mathrm{TF}})^2} \frac{\cos(2k_F d)}{k_F d^3} \tag{36}$$
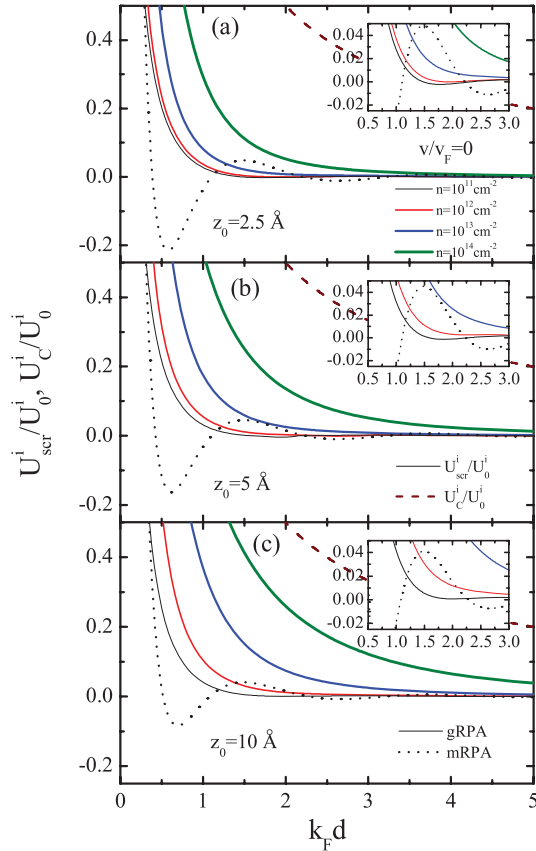
FIG. 7. (Color online) The total screened interaction energy U_{scr}^i, normalized by $U_0^i = Z^2 e^2 k_F$ with $k_F = \sqrt{\pi n}$, is shown as a function of the reduced interionic separation $k_F d$ for two static ions of equal charges Ze, adsorbed at equal distances above free graphene: $z_0 = 2.5$ Å (a), 5 Å (b), and 10 Å (c) for four graphene doping densities: $n = 10^{11}$ cm^{-2} (thin solid black lines), $n = 10^{12}$ cm^{-2} [thin solid gray (red) lines], $n = 10^{13}$ cm^{-2} [medium solid gray (blue) lines], and $n = 10^{14}$ cm^{-2} [thick solid gray (olive) lines]. The case of ion-ion interaction energy above a free massive 2DEG with the electron density $n = 10^{11}$ cm^{-2} is shown by black dotted lines, and the bare Coulomb interaction U_C^i is shown by the dashed gray (wine) lines.

for $z_0 \ll k_F^{-1} \ll d$, exhibiting an amplitude that decays with d at essentially the same rate as the TF interaction.

Because of the importance of the interadatom electrostatic interactions mediated by a m2DEG,[7,8] we also show in Fig. 7 the total screened interaction energy for a free m2DEG with the electron density $n = 10^{11}$ cm^{-2} and with the effective mass $m_{eff} = 2\hbar\sqrt{\pi n}/(m_0 v_F)$, where m_0 is the free-electron mass and v_F is graphene's Fermi speed. This choice of m_{eff} ensures that the m2DEG has the same TF wave number as graphene so that, by using the same normalization as in the results for graphene in Fig. 7, the two systems would have identical TF interaction energies. As a consequence, direct comparison of the curves in Fig. 7 for graphene with $n = 10^{11}$ cm^{-2} with those for m2DEG clearly shows that the latter system exhibits much more pronounced FOs in the ion-ion interaction energy. This is expected because the asymptotic form of FOs for a m2DEG,[2]

$$U_{FO}^i \propto -\frac{Z^2 e^2 q_{TF}}{(2K_F + q_{TF})^2} \frac{\sin(2K_F d)}{d^2}, \qquad (37)$$

where $K_F = \sqrt{2\pi n}$, has an amplitude of oscillations that exhibits a slower decay with d than the amplitude in Eq. (36) for graphene. The observed difference in FOs may be related to the observations of ordering in the layers of ionized adatoms on surfaces with m2DEG,[7,8] and the lack thereof in the analogous systems on graphene.[15,16]

Finally, for intrinsic graphene above a substrate with zero gap and with static dielectric constant ϵ_{sub}, the total screened interaction energy between two coadsorbed ions is simply given by the Coulomb repulsion, screened by the interaction of ions with each other's image in the plane of graphene,

$$U_{scr}^i = \frac{Z^2 e^2}{d} + \frac{Z^2 e^2}{\sqrt{d^2 + (2z_0)^2}}\left(\frac{1}{\epsilon_{eff}^0} - 1\right), \qquad (38)$$

where $\epsilon_{eff}^0 = \epsilon_{bg}^0 + \pi r_s/2$ is an effective static dielectric constant of the system with $\epsilon_{bg}^0 = (\epsilon_{sub} + 1)/2$.[31,33] In order to compare this simple result in the case of free graphene with those shown for doped graphene in Fig. 7(b), we show in Fig. 10(a) the total screened interaction energy for static ions U_{scr}^i normalized by $U_C^i = Z^2 e^2/d$ as a function of the reduced interionic separation $d/(2z_0)$ with $z_0 = 5$ Å for several doping densities n. One may conclude that the screening efficiency of intrinsic graphene is comparable with that of doped graphene with the lowest charge carrier density of $n = 10^{11}$ cm^{-2} in Fig. 10(a) for interionic separations $d \lesssim 2z_0$. However, the screening ratio U_{scr}^i/U_C^i for intrinsic graphene approaches a constant value of $1/\epsilon_{eff}^0 = 1/(1 + \pi r_s/2) \approx 0.225$ at large separations $d \gg 2z_0$, whereas this ratio vanishes for doped graphene at finite separations that depend on charge carrier density $d \gtrsim 2/k_F$, confirming that screening efficiency of doped graphene increases with increasing n.

2. Two static dipoles

Moving on to a more complex problem of the coadsorption of dipolar molecules on doped graphene,[9] we use Eqs. (30) and (32) to evaluate the total screened interaction energy U_{scr}^d for a static pair of point dipoles having the dipole moments $\boldsymbol{\mu}_1$ and $\boldsymbol{\mu}_2$ of equal magnitudes $\|\boldsymbol{\mu}_1\| = \|\boldsymbol{\mu}_2\| = \mu$, which are placed on free graphene at equal distances z_0, and are separated by a relative position vector $\mathbf{d}$. The results for U_{scr}^d are normalized by $U_0^d = \mu^2 k_F^3$ and are shown in Fig. 8 as a function of the reduced interdipole separation $k_F d$ for $z_0 = 5$ Å, for several doping densities n, and for several dipole moment orientations: (a) both dipoles perpendicular to graphene and parallel to each other, (b) both dipoles parallel to graphene, parallel to $\mathbf{d}$, and antiparallel to each other, and (c) both dipoles parallel to graphene, perpendicular to $\mathbf{d}$, and parallel to each other. Also shown in Fig. 8 are the bare Coulombic interaction energies between the dipoles for those three configurations U_C^d based on Eq. (32).

Noting that the configuration (a) is most likely to occur in the coadsorption of dipolar molecules on a surface, one notices in Fig. 8(a) that the screened interaction energy is repulsive and, in fact, stronger than the corresponding bare Coulombic interaction at large distances d for all doping densities. This apparent "antiscreening" by graphene may be rationalized by noting that the total interaction energy for two dipoles perpendicular to graphene is determined by the first terms in
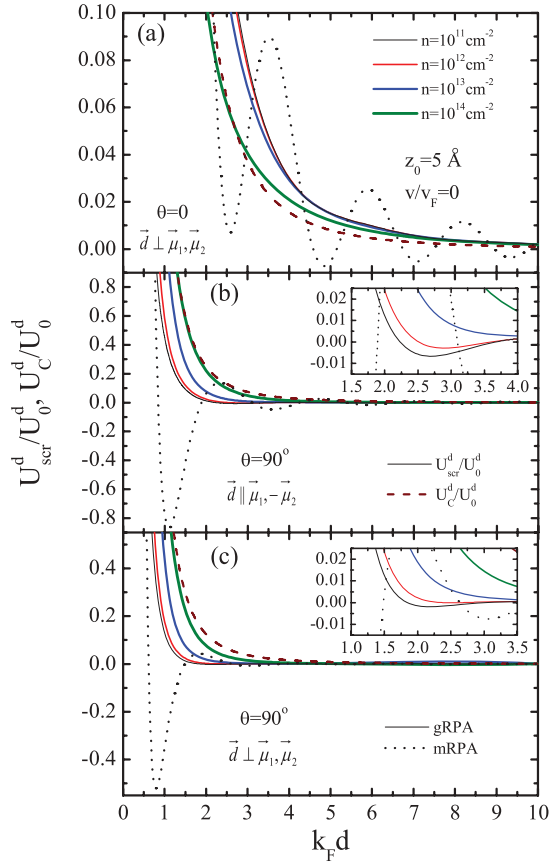
FIG. 8. (Color online) The total screened interaction energy U_{scr}^d, normalized by $U_0^d = \mu^2 k_F^3$ with $k_F = \sqrt{\pi n}$, is shown as a function of the reduced interdipole separation $k_F d$ for two static dipoles with equal magnitudes of the dipole moments μ, which are adsorbed at equal distances $z_0 = 5$ Å from free graphene for four graphene doping densities: $n = 10^{11}$ cm^{-2} (thin solid black lines), $n = 10^{12}$ cm^{-2} [thin solid gray (red) lines], $n = 10^{13}$ cm^{-2} [medium solid gray (blue) lines], and $n = 10^{14}$ cm^{-2} [thick solid gray (olive) lines], for three dipole orientations with respect to the interdipole relative position vector **d**: (a) both dipoles perpendicular to graphene and parallel to each other, (b) both dipoles parallel to graphene, parallel to **d**, and antiparallel to each other, and (c) both dipoles parallel to graphene, perpendicular to **d**, and parallel to each other. The case of the dipole-dipole interaction energy above a free massive 2DEG with the electron density $n = 10^{11}$ cm^{-2} is shown by black dotted lines, and the bare Coulombic interactions U_C^d are shown by the dashed gray (wine) lines.

Eqs. (30) and (32). A careful asymptotic analysis of the TF approximation for the total interaction energy in this dipole configuration shows that the leading term is $U_{int}^d \propto 2\mu^2/d^3$ for $z_0 \ll q_{TF}^{-1} \ll d$, i.e., *twice* the bare Coulombic repulsion between the dipoles with the same configuration in free space $U_C^d = \mu^2/d^3$. This is in qualitative agreement with the findings of Ref. 9 for the long-ranged dipole-dipole repulsion on a metal surface with m2DEG.

On the other hand, the other two configurations for a pair of static dipoles, shown in Figs. 8(b) and 8(c), could be of interest for coadsorption of nanoparticles on graphene,[21] or polar molecules on metal surfaces.[22] One notices in Figs. 8(b) and 8(c) that graphene does provide screening of the corresponding bare Coulombic interaction energies,

given by $U_C^d = 2\mu^2/d^3$ and $U_C^d = \mu^2/d^3$, respectively, which is not as substantial as the screening seen in Fig. 7 for a pair of static ions. An asymptotic analysis of the TF approximation for the total dipole-dipole interaction energy for the configurations (b) and (c) yields much shorter-ranged expressions $U_{int}^d \propto 12\mu^2/(q_{TF}^2 d^5)$ and $U_{int}^d \propto 3\mu^2/(q_{TF}^2 d^5)$ for $z_0 \ll q_{TF}^{-1} \ll d$, respectively, than the above expression for the configuration (a). Moreover, the insets of Figs. 8(b) and 8(c) exhibit shallow minima at lower doping densities due to FOs in those two configurations, which are not seen in the configuration (a). This may be rationalized by considering the asymptotic behavior of the FO terms in the corresponding expressions for the dipole-dipole interactions for all three configurations, which are simply proportional to those given in Eq. (36) for FOs in the ion-ion interaction, and are scaled by the factor $[\mu q_{TF}/(Ze)]^2$ for dipoles. With the amplitude of FOs retaining the $\sim d^{-3}$ dependence on distance from Eq. (36), one expects that FOs in the dipole-dipole interaction would be absorbed by the dominant long-ranged Columbic repulsion in the configuration (a), but would show up in the configurations (b) and (c) with the much shorter-ranged TF asymptotics.

We also show in Fig. 8 the screened dipole-dipole interaction for a free m2DEG, evaluated with the same parameters as those used in Fig. 7 for the m2DEG case. One notices in Fig. 8 that FOs in this system give rise to prominent minima in the dipole-dipole interaction energy for all three configurations, with amplitudes that far exceed those seen for graphene with the same density as the m2DEG, $n = 10^{11}$ cm^{-2}. Such strong manifestation of FOs, especially for two dipoles perpendicular to m2DEG, is at variance with the observations in Ref. 9, which may be explained by a possibly strong suppression of FOs in the m2DEG due to the screening by a metallic substrate.[19]

Finally, it is worth mentioning that the statically screened dipole-dipole interaction may be evaluated analytically for intrinsic graphene above a substrate with zero gap and with static dielectric constant ϵ_{sub} by using Eqs. (30) and (32) with the coefficients V_k from Eq. (31) given in the form $V_k = W_k[d^2 + (2z_0)^2]^{-5/2}(1/\epsilon_{eff}^0 - 1)$, where $W_0 = 8z_0^2 - d^2$, $W_1 = 6z_0 d$, and $W_2 = 3d^2$. In order to compare this simple result in the case of free graphene with those shown for doped graphene in Fig. 8(a), we show in Fig. 10(b) the total screened interaction energy for static dipoles with dipole moments perpendicular to graphene, U_{scr}^d, normalized by $U_C^d = \mu^2/d^3$, as a function of the reduced interdipole separation $d/(2z_0)$ with $z_0 = 5$ Å, for several doping densities n. One may conclude that the screening efficiency of intrinsic graphene is comparable with that of doped graphene for all charge carrier densities in Fig. 10(b) for separations $d \lesssim 2z_0$. However, the screening ratio U_{scr}^d/U_C^d for intrinsic graphene approaches a constant value of $2 - 1/\epsilon_{eff}^0 \approx 1.775$ at large separations $d \gg 2z_0$, whereas this ratio for doped graphene tends to oscillate about the value 2 at finite separations $d \gtrsim 2/k_F$.

3. *Moving pair of ions*

Relative motion of ion fragments during Coulomb explosion of a molecule with an incident velocity **v** may be treated as adiabatic in the frame of reference that moves with the same velocity, but the dynamics of the Coulomb explosion

on a slow time scale in that frame is necessarily affected by the dynamical effects in the screened interaction energy between the ion fragments when $v = \|\mathbf{v}\|$ is comparable to v_F.[55–57,75] Hence, we evaluate the total screened interaction energy U_{scr}^i from Eq. (27) for two ions with equal charges Ze, moving parallel to free, doped graphene with equal velocities at equal distances z_0 from graphene, and with a relative position vector $\mathbf{d}$. The results for a randomly oriented $\mathbf{d}$ are normalized by $U_0^i = Z^2 e^2 k_F$ and are displayed by the solid lines in Fig. 9 as a function of the reduced separation $k_F d$ between the ions, for the speed of $v = 2v_F$, for three distances z_0, and for four doping densities n. One notices that oscillations develop in the interaction energy, which are more pronounced at shorter distances z_0 and lower densities n (within the given normalization). A comparison with the bare Coulomb interaction, also displayed in Fig. 9, shows
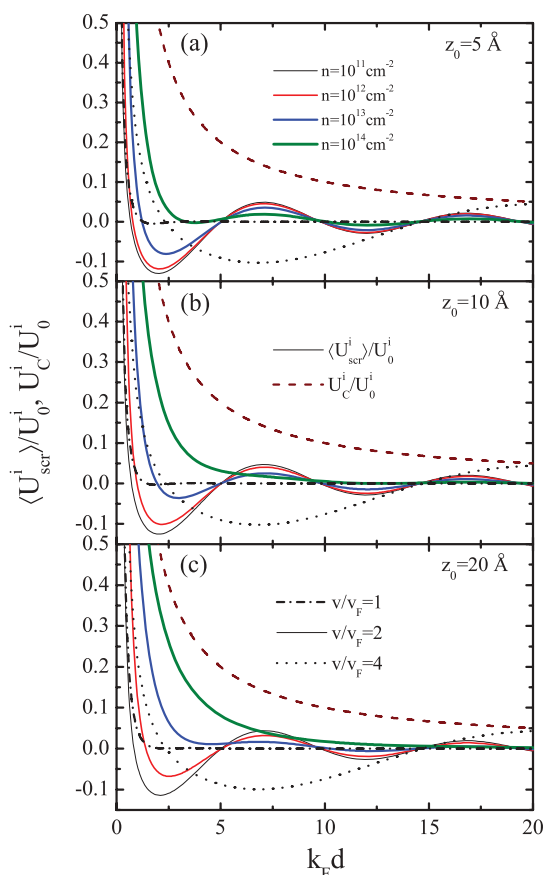
FIG. 9. (Color online) The total screened interaction energy $\langle U_{scr}^i \rangle$, normalized by $U_0^i = Z^2 e^2 k_F$ with $k_F = \sqrt{\pi n}$, is shown as a function of the reduced interionic separation $k_F d$ for two ions of equal charges Ze, moving parallel to free graphene at the speed $v = 2v_F$ (solid lines) with randomly oriented interionic axis and at equal distances above free graphene: $z_0 = 5$ Å (a), 10 Å (b), and 20 Å (c) for four doping densities: $n = 10^{11}$ cm^{-2} (black lines: thin solid, dotted, and dashed-dotted), $n = 10^{12}$ cm^{-2} [thin solid gray (red) lines], $n = 10^{13}$ cm^{-2} [medium solid gray (blue) lines], and $n = 10^{14}$ cm^{-2} [thick solid gray (olive) lines]. Also shown is the normalized $\langle U_{scr}^i \rangle$ for two ions moving at the speeds $v = v_F$ (dashed-dotted black lines) and $v = 4v_F$ (dotted black lines), both for doping density of $n = 10^{11}$ cm^{-2}. The bare Coulomb interaction U_C^i is shown by the dashed gray (wine) lines.

that the screening by graphene at short and intermediate separations is still effective at such high speeds for all densities. As a consequence, the dynamical effects in screening of the interaction energy between the two ions may be responsible for slowing down the Coulomb explosion, whereas the oscillations in that energy may even give rise to the so-called wake-riding bound states for the correlated ions, as was observed in solids[75] and on surfaces.[56,57] In that context, it may be worthwhile examining the actual values of the screened interaction energy at the first minima U_{min}^1 seen, e.g., in Fig. 9(a) with $z_0 = 5$ Å and $v = 2v_F$ for two protons ($Z = 1$), where we find the coordinates (d_{min}, U_{min}^1) of those minima to be (35.7 nm, -10.5 meV), (11.6 nm, -30.4 meV), (4.2 nm, -65.6 meV), and (2.1 nm, -6.9 meV) for $n = 10^{11}$, 10^{12}, 10^{13}, and 10^{14} cm^{-2}, respectively. Moreover, by inverting the signs of the curves shown in Fig. 9, one would obtain a dynamically screened interaction energy between an electron and a proton that are comoving above graphene, whereby a wake-riding bound state of the electron may occur around the electron-proton separations where the first peaks arise in the curves seen in Fig. 9 (at $d \approx 7/k_F$ for $v = 2v_F$).[76]

In Fig. 9, we also show the total screened interaction energy for two ions moving at the speeds $v = v_F$ and $v = 4v_F$ at the three distances z_0 for graphene's doping density of $n = 10^{11}$ cm^{-2}. By a comparison with the curves at $v = 2v_F$ for the same doping density, one notices that the period of oscillations in the screened interaction energy and the rate of their damping with increasing separation d strongly depend on the speed v of the comoving ions in such a manner that the period increases and the damping rate decreases with increasing v (notice how the amplitude of the oscillations at $v = 4v_F$ becomes comparable with the bare Coulomb interaction at the largest separation shown in Fig. 9, $d = 20/k_F$). Thus, v arises as yet another (in addition to n) parameter that could be used to control the wake-riding states. However, noting that the oscillations seen in Fig. 9 are directly related to the wake effect in the ion-induced charge in graphene, which is seen in Fig. 2(b) and was previously studied in detail,[35] we emphasize that the rate of damping of those oscillations with the increasing d may be expected to be substantially higher if a finite damping constant γ is introduced in the dielectric function for graphene.[35]

Considering the case of intrinsic graphene above a substrate with zero gap and with static dielectric constant ϵ_{sub}, we note that oscillations in the total screened interaction energy between two comoving ions vanish for all speeds. In that case, the total screened interaction energy with randomly oriented interionic axis $\langle U_{scr}^i \rangle$ is given by the right-hand side of Eq. (38) with $\epsilon_{eff}(0)$ replaced by a velocity-dependent effective dielectric constant $\epsilon_{eff}(v)$, which was discussed in Fig. 5 of Ref. 33. In order to compare this simple result in the case of free intrinsic graphene with those shown for doped graphene in Fig. 9(a), we show in Fig. 10(c) the total screened interaction energy for two comoving ions with $v = 2v_F$, $\langle U_{scr}^i \rangle$, normalized by $U_C^i = Z^2 e^2/d$, as a function of the reduced interionic separation $d/(2z_0)$ with $z_0 = 5$ Å, for several doping densities n. One may conclude that the screening efficiency of intrinsic graphene is comparable with that of doped graphene with the lowest charge carrier density of $n = 10^{11}$ cm^{-2} in Fig. 10(c) for interionic separations
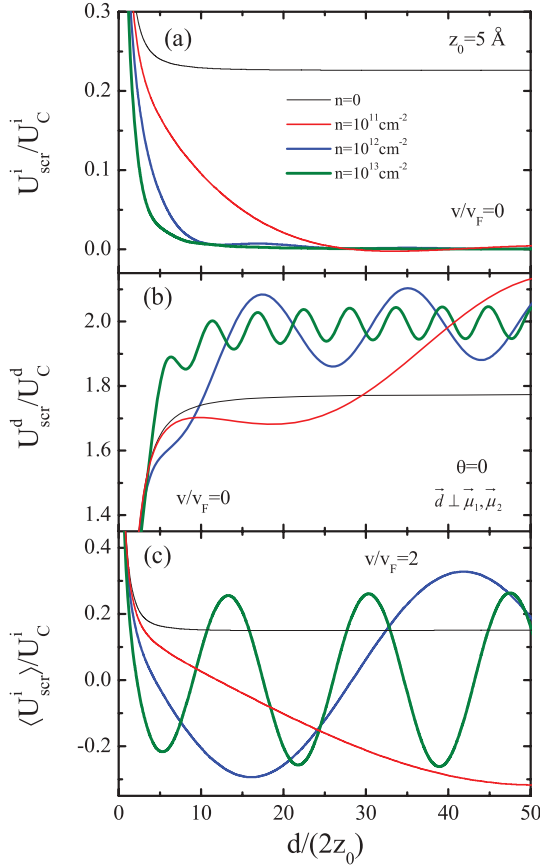
FIG. 10. (Color online) The dependence on the reduced interparticle separation $d/(2z_0)$ with $z_0 = 5$ Å is shown for the total screened interaction energy between (a) two static ions $U_{\text{scr}}^{\text{i}}$ normalized by $U_{\text{C}}^{\text{i}} = Z^2 e^2/d$, (b) two static dipoles $U_{\text{scr}}^{\text{d}}$ normalized by $U_{\text{C}}^{\text{d}} = \mu^2/d^3$, and (c) two ions moving at the speed $v = 2v_F$ with randomly oriented interionic axis $\langle U_{\text{scr}}^{\text{i}} \rangle$, normalized by $U_{\text{C}}^{\text{i}} = Z^2 e^2/d$, for free intrinsic graphene $n = 0$ (thin solid black lines), and for three doping densities: $n = 10^{11}$ cm^{-2} [thin solid gray (red) lines], $n = 10^{12}$ cm^{-2} [medium solid gray (blue) lines], and $n = 10^{13}$ cm^{-2} [thick solid gray (olive) lines].

$d \lesssim 2z_0$. However, the screening ratio $U_{\text{scr}}^{\text{i}}/U_{\text{C}}^{\text{i}}$ for intrinsic graphene approaches a constant value of $1/\epsilon_{\text{eff}}(2v_F) \approx 0.150$ at large separations $d \gg 2z_0$, whereas this ratio for doped graphene undergoes large-amplitude oscillates about zero at finite separations $d \gtrsim 2/k_F$.

On the other hand, the interference effects in energy loss to the underlying medium due to the spatial correlation of ion fragments in Coulomb explosion may be responsible for an enhancement or reduction of the stopping of correlated ion fragments.[55–57,75] The corresponding vicinage effect ratio $R = (d\mathcal{E}/dt)_{\text{vic}}/[2(d\mathcal{E}/dt)_{\text{ion}}]$ is evaluated from Eq. (28) for two ions with equal charges, moving parallel to a free graphene with equal velocities **v** at equal distances z_0 for several orientational configurations of the interionic axis **d** with respect to **v**. We first consider in Fig. 11 the case of intrinsic graphene for ions with $v > v_F$, where R may actually be obtained in an analytic form as a function of the reduced interionic separation $d/(2z_0)$ for **d** parallel to **v** (directed motion of ion fragments), **d** perpendicular to **v**, and randomly oriented **d**. One notices that R generally decays from
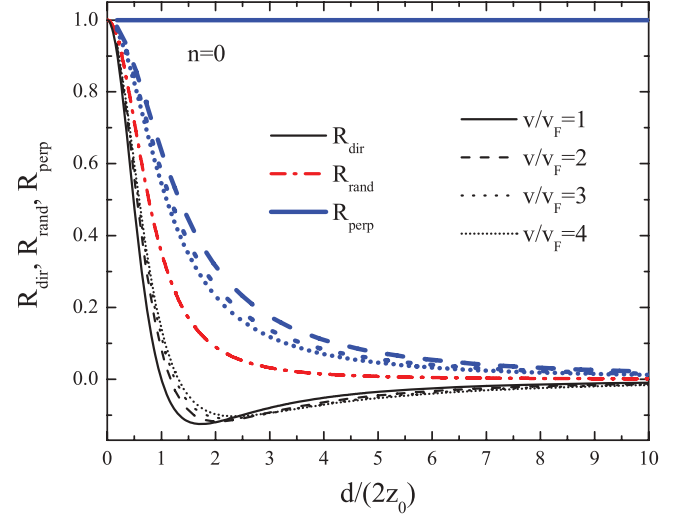
FIG. 11. (Color online) The energy-loss ratio $R = (d\mathcal{E}/dt)_{\text{vic}}/[2(d\mathcal{E}/dt)_{\text{ion}}]$ displays vicinage effects as a function of the reduced interionic separation $d/(2z_0)$ for two ions with equal charges, moving parallel to a free, intrinsic graphene (doping density $n = 0$) at equal distances z_0 from graphene with four speeds: $v = v_F$ (solid lines), $2v_F$ (dashed lines), $3v_F$ (dotted lines), and $4v_F$ (short dotted lines) for three orientations of the interionic axis: parallel to the direction of motion (R_{dir}, thin black lines), perpendicular to the direction of motion [R_{perp}, thick gray (blue) lines], and random orientations [R_{rand}, dashed-dotted gray (red) line for all four speeds].

a maximum $R = 1$ at $d = 0$ towards zero at $d \gg 2z_0$, but does so in a manner that strongly depends on the orientation and speed v. As expected, the dependence of R_{dir} for directed motion on d is nonmonotonic, showing that the trailing ion fragment may experience significantly reduced energy loss by simply coasting in the wake of the leading fragment, so that the total energy loss may even be reduced compared to the total energy loss of two independent fragments. In the case of perpendicular direction, the two ion fragments always experience increased energy loss, $R_{\text{perp}} > 0$, whereas the case of random orientations always lies between the other two cases and is, in fact, given by $R_{\text{rand}} = [1 + d^2/(2z_0)^2]^{-3/2}$, corresponding to the $v \to \infty$ limit of the results for either the directed or perpendicular configurations.

Finally, we study in Fig. 12 the effects of finite graphene doping density n on the ratio R as a function of the reduced separation $k_F d$ between two ions for two speeds $v = v_F$ and $2v_F$, and for two cases corresponding to a directed motion and random orientations of the interionic axis. One notices that, in both cases, higher speed and higher density n give rise to a more pronounced quasioscillatory dependence of the ratio R on the distance d. For the highest density shown in Fig. 12, $n = 10^{13}$ cm^{-2}, those oscillations are surprisingly persistent at large distances d, even for random orientations, which may be attributed to the interferences in the energy loss arising due to plasmon excitations in heavily doped graphene. On the other hand, considering the lowest density shown in Fig. 12, $n = 10^{11}$ cm^{-2}, one sees that both R_{dir} and R_{rand} are close to the corresponding results in Fig. 11 (where $n = 0$) for $v = 2v_F$, but not for $v = v_F$, showing that interesting
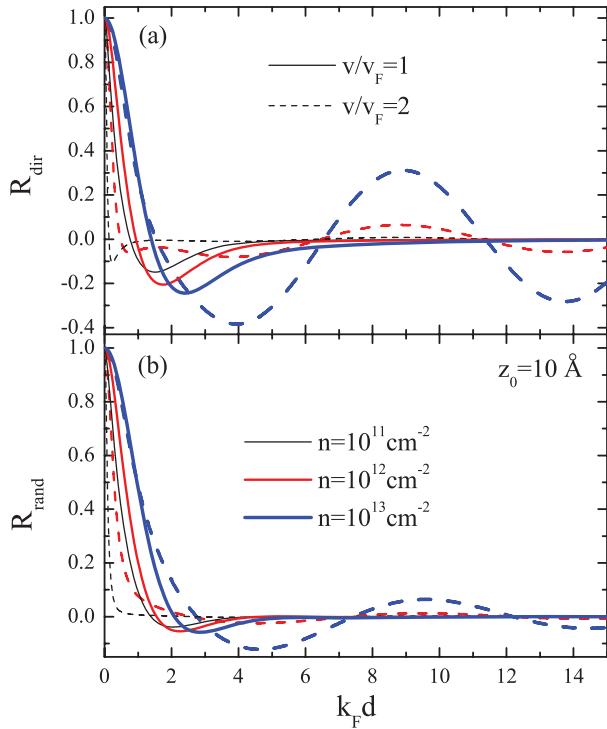
FIG. 12. (Color online) The energy-loss ratio $R = (d\mathcal{E}/dt)_{\text{vic}}/[2(d\mathcal{E}/dt)_{\text{ion}}]$ displays vicinage effects as a function of the reduced interionic separation $k_F d$, where $k_F = \sqrt{\pi n}$, for two ions with equal charges, moving parallel to a free graphene at equal distances $z_0 = 10$ Å with two speeds: $v = v_F$ (solid lines) and $v = 2v_F$ (dashed lines) for three doping densities: $n = 10^{11}$ cm^{-2} (thin black lines), $n = 10^{12}$ cm^{-2} [medium gray (red) lines], and $n = 10^{13}$ cm^{-2} [thick gray (blue) lines] for two orientations of the interionic axis: parallel to the direction of motion (R_{dir}, panel a) and random orientations (R_{rand}, panel b).

vicinage effects in the energy loss may occur due to doping when the ion speed matches the phase velocity in the (q, ω) plane of graphene's polarization function that corresponds to the boundary between the interband and intraband SPEs.[18,31]

IV. CONCLUDING REMARKS

We have studied polarization of the π-electron system in a single-layer graphene by the spatially correlated external charges, which either move over the graphene at a finite speed, or are statically adsorbed on graphene. A point dipole model is used to discuss (a) nondissociative grazing scattering of a molecule with permanent dipole moment from graphene, and (b) electrostatic interaction between two dipolar molecules physisorbed on graphene. Two point ions are used as a model to discuss (a) the comoving ion fragments during Coulomb explosion of a grazingly scattered diatomic molecule from graphene, and (b) electrostatic interaction in the coadsorption of, e.g., alkali-metal atoms on graphene.

Among the many parameters in this study, we have concentrated on the effects of graphene doping with finite-equilibrium charge carrier density n, and we found that the interaction of graphene with all the above model systems may be effectively controlled by n. While the response of graphene's

π electrons was mostly described by a dielectric function for free graphene within the random phase approximation with zero damping, the effect of finite damping and the effect of a polar substrate that supports a surface phonon were also briefly discussed. Moreover, several comparisons of results were made by replacing graphene with a 2DEG with a parabolic energy band that was also described within the random phase approximation.

For a moving dipole, we obtained the self-energy (image potential) and calculated the image force and the stopping force in the direction of motion, and we showed that there also exists a dissipative force perpendicular to the direction of motion. Using suitable scaling factors, we demonstrated qualitative similarity between the stopping and the image forces on a moving dipole and these forces on a moving ion, with a notable exception that the image force on the dipole may become repulsive at high enough doping densities of graphene, large enough distances from graphene, and high enough dipole speeds. Moreover, we showed that the wake effect in the induced charge density due to a moving dipole may be asymmetric with respect to the direction of motion. We have also evaluated a torque on the moving dipole, with components that consist of both the dissipative and conservative interactions, showing strong propensity of the moving molecule for rotation due to the dynamic polarization of graphene.

For a static pair of ions with equal charges Ze that are coadsorbed on graphene, we have evaluated the screened interaction energy as a function of the interionic separation d, and showed that doping of graphene provides significant screening of the Coulomb interaction, giving rise to a repulsive interaction of the form $Z^2 e^2/(q_{\text{TF}}^2 d^3)$ at large separations $d \gg q_{\text{TF}}^{-1}$, where q_{TF} is graphene's Thomas-Fermi wave number. Shallow minima were found in the interaction energy at finite separations $d \sim 2/k_F$, where $k_F = \sqrt{\pi n}$ is graphene's Fermi wave number, which were attributed to Friedel oscillations. A comparison with the screened ion-ion interaction on a comparable 2DEG showed that this system exhibits much more prominent Friedel oscillations than graphene.

For a static pair of dipoles with equal dipole moments of magnitude μ that are coadsorbed on graphene, the screened interaction energy was found to have the form $\mu^2/(q_{\text{TF}}^2 d^5)$ at large dipole-dipole separations $d \gg q_{\text{TF}}^{-1}$ in cases when both dipoles are parallel to graphene. In those cases, we also found shallow minima in the dipole-dipole interaction energy at finite separations due to Friedel oscillations, which are much less prominent than Friedel oscillations on a comparable 2DEG. On the other hand, when both dipoles are perpendicular to graphene, we found a strongly repulsive interaction, which approaches $2\mu^2/d^3$ at large separations, i.e., twice the Coulombic repulsion between the dipoles in free space, which may be described as antiscreening due to the dipoles' image interaction with graphene.

The above findings for the static pairs of ions and dipoles show that (a) electrostatic interaction energy between the adsorbed species may be efficiently controlled by graphene's doping density, (b) long-range ordering due to Friedel oscillations is less likely on graphene than on a surface with a 2DEG, (c) clustering of the ionic species on graphene may be possible at higher doping densities due to reduction in

the range of repulsive interaction, but (d) clustering of the dipolar species seems unlikely due to antiscreening of the dipole-dipole interaction in the presence of graphene.

For a pair of ions that are comoving at a speed in excess of graphene's Fermi speed v_F, our calculations of the dynamically screened interaction energy showed prominent oscillations with the interionic separation d, which are directly related to the ion wake effect in the polarization of graphene. Such oscillations could give rise to dynamically induced bound (or wake-riding) states of the comoving ions, which may be controlled by graphene doping and/or by ions' speed. In addition, an analysis of the interference, or the vicinage effects in the energy loss to graphene due to the comoving pair of ions with equal charges, showed that the total energy loss may become close to four times the loss of an isolated ion at the same speed for very short interionic separations d, but may also become less than twice the loss of an isolated ion for finite separations d that depend on the speed of ions and the doping density of graphene. Such reduction of the energy loss suggests that a wake-riding state of two ions may be the most energetically favorable mode of propagation of correlated charges above graphene.

Regarding the possible improvements of the model system, we note that we found indications that screening by a substrate may play an important role in the interaction energy among correlated charges, especially in the static coadsorption on graphene (and 2DEG) in the presence of a metallic substrate, as well as in the dynamic regime at low propagation speeds when excitations of surface phonons in a polar substrate may play a role in the energy loss of correlated charges. Finally, probably the most intriguing aspect of the problem at hand is the regime close to a neutral, or intrinsic graphene, where a system of electron-hole puddles usually develops on graphene. In such a situation, screening of the interaction between charges that are separated by distances comparable to the size of those puddles would require substantial modifications of the present model, which will be tackled in the future.

ACKNOWLEDGMENTS

APPENDIX: WAKE EFFECT

An expression for the Fourier transform (FT) of the charge density $n_{\text{ind}}(\mathbf{r},t)$, induced by an external charge distribution $\rho(\mathbf{R},t)$, follows from the definition of graphene's polarization function $\widetilde{n}_{\text{ind}}(\mathbf{q},\omega) = e\Pi(\mathbf{q},\omega)\widetilde{\Phi}_{\text{tot}}(\mathbf{q},z,\omega)|_{z=0}$, where the FT of the total potential is given in terms of the FT of the total Green's function by

$$\widetilde{\Phi}_{\text{tot}}(\mathbf{q},z,\omega) = \int dz' \int_{-\infty}^{\infty} dt' \, \widetilde{G}(\mathbf{q},z,z';\omega)\widetilde{\rho}(\mathbf{q},z',\omega). \quad (A1)$$

One may then show that

$$n_{\text{ind}}(\mathbf{r},t) = e \int d^3\mathbf{R}' \int_{-\infty}^{\infty} dt' H(\mathbf{R},\mathbf{R}';t-t')|_{z=0}\, \rho(\mathbf{R}',t'), \tag{A2}$$

where $H(\mathbf{R},\mathbf{R}';t-t') = H(\mathbf{r}-\mathbf{r}',z,z',t-t')$ is an inverse FT of the product $\Pi(\mathbf{q},\omega)\widetilde{G}(\mathbf{q},z,z';\omega)$.

By using the charge density $\rho(\mathbf{R},t) = Ze\,\delta[\mathbf{R}-\mathbf{R}_0(t)]$ for a point ion that moves parallel to graphene along the trajectory $\mathbf{R}_0(t) = \{\mathbf{v}t,z_0\}$, and referring to Eqs. (1) and (2), one may show that the induced charge density is stationary in the moving frame attached to the ion, and is given by[35]

$$n_{\text{ind}}(\mathbf{r},t) \equiv n_{\text{ind}}^{\text{i}}(\boldsymbol{\xi},z_0)$$
$$= Z \int \frac{d^2\mathbf{q}}{(2\pi)^2}\, e^{-qz_0}e^{i\mathbf{q}\cdot\boldsymbol{\xi}}\left[1 - \frac{\epsilon_{\text{bg}}(q,\mathbf{q}\cdot\mathbf{v})}{\epsilon(q,\mathbf{q}\cdot\mathbf{v})}\right], \quad (A3)$$

where $\boldsymbol{\xi} \equiv \mathbf{r} - \mathbf{v}t$.

If one replaces the density $\rho(\mathbf{R},t)$ in Eq. (A2) with $\rho_{\text{dip}}(\mathbf{R},t) = -\boldsymbol{\mu}\cdot\nabla_{\mathbf{R}}\,\delta[\mathbf{R}-\mathbf{R}_0(t)]$, characteristic of a point dipole with the moment $\boldsymbol{\mu}$ that moves along the trajectory $\mathbf{R}_0(t) = \{\mathbf{v}t,z_0\}$, one may show that then

$$n_{\text{ind}}(\mathbf{r},t) = e\int_{-\infty}^{\infty} dt'\, \boldsymbol{\mu}\cdot\nabla_{\mathbf{R}'} H(\mathbf{R},\mathbf{R}';t-t')|_{z=0,\,\mathbf{R}'=\mathbf{R}_0(t')}. \tag{A4}$$

Hence, the charge density induced in graphene by a dipole may be related to the one induced by the ion in Eq. (A3) via $n_{\text{ind}}^{\text{d}}(\mathbf{X}) = (Ze)^{-1}\boldsymbol{\mu}\cdot\nabla_{\mathbf{X}}n_{\text{ind}}^{\text{i}}(\mathbf{X})$, where $\mathbf{X} \equiv \{\boldsymbol{\xi},z_0\} = \{x-vt,y,z_0\}$ for particles moving in the direction of the x axis.

---

*zmiskovi@math.uwaterloo.ca

[1] A. H. Castro Neto, F. Guinea, N. M. Peres, K. S. Novoselov, and A. K. Geim, Rev. Mod. Phys. **81**, 109 (2009).

[2] S. Das Sarma, S. Adam, E. H. Hwang, and E. Rossi, Rev. Mod. Phys. **83**, 407 (2011).

[3] Q. Li, E. H. Hwang, E. Rossi, and S. Das Sarma, Phys. Rev. Lett. **107**, 156601 (2011).

[4] J. Yan and M. S. Fuhrer, Phys. Rev. Lett. **107**, 206601 (2011).

[5] K. M. McCreary, K. Pi, A. G. Swartz, W. Han, W. Bao, C. N. Lau, F. Guinea, M. I. Katsnelson, and R. K. Kawakami, Phys. Rev. B **81**, 115453 (2010).

[6] P. Han and P. S. Weiss, Surf. Sci. Rep. **67**, 19 (2012).

[7] N. Knorr, H. Brune, M. Epple, A. Hirstein, M. A. Schneider, and K. Kern, Phys. Rev. B **65**, 115420 (2002).

[8] H. Bentmann, A. Buchter, and F. Reinert, Phys. Rev. B **85**, 121412(R) (2012).

[9] T. Yokoyama, T. Takahasi, K. Shinozaki, and M. Okamoto, Phys. Rev. Lett. **98**, 206102 (2007).

[10] T. O. Wehling, M. I. Katsnelson, and A. I. Lichtenstein, Chem. Phys. Lett. **476**, 125 (2009).

[11] K. T. Chan, J. B. Neaton, and M. L. Cohen, Phys. Rev. B **77**, 235430 (2008).

[12] R. R. Q. Freitas, R. Rivelino, F. de Brito Mota, and C. M. C. de Castilho, J. Phys. Chem. A **115**, 12348 (2011).

[13] J. H. Chen, C. Jang, S. Adam, M. S. Fuhrer, E. D. Williams, and M. Ishigami, Nat. Phys. **4**, 377 (2008).

[14] S. Adam, E. H. Hwang, V. M. Galiskii, and S. Das Sarma, Proc. Natl. Acad. Sci. USA **104**, 18392 (2007).

[15] J. Renard, M. B. Lundeberg, J. A. Folk, and Y. Pennec, Phys. Rev. Lett. **106**, 156101 (2011).

[16] C.-L. Song, B. Sun, Y.-L. Wang, Y.-P. Jiang, L. Wang, K. He, X. Chen, P. Zhang, X.-C. Ma, and Q.-K. Xue, Phys. Rev. Lett. **108**, 156803 (2012).

[17] V. V. Cheianov and V. I. Falko, Phys. Rev. Lett. **97**, 226801 (2006).

[18] B. Wunsch, T. Stauber, F. Sols, and F. Guinea, New J. Phys. **8**, 318 (2006).

[19] V. M. Silkin, I. A. Nechaev, E. V. Chulkov, and P. M. Echenique, Surf. Sci. **600**, 3875 (2006).

[20] M. Urbakh and J. Klafter, J. Phys. Chem. **97**, 3344 (1993).

[21] D. V. Talapin, E. V. Shevchenko, C. B. Murray, A. V. Titov, and P. Kral, Nano Lett. **7**, 1213 (2007).

[22] A. Kokalj, Phys. Rev. B **84**, 045418 (2011).

[23] Y. Liu, R. F. Willis, K. V. Emtsev, and Th. Seyller, Phys. Rev. B **78**, 201403(R) (2008).

[24] Y. Liu and R. F. Willis, Phys. Rev. B **81**, 081406(R) (2010).

[25] T. Langer, J. Baringhaus, H. Pfnür, H. W. Schumacher, and C. Tegenkamp, New J. Phys. **12**, 033017 (2010).

[26] T. Langer, D. F. Förster, C. Busse, T. Michely, H. Pfnür, and C. Tegenkamp, New J. Phys. **13**, 053006 (2011).

[27] M. A. Romero, A. Iglesias-Garcia, and E. C. Goldberg, Phys. Rev. B **83**, 125411 (2011).

[28] M. A. Romero, A. Iglesias-Garcia, and E. C. Goldberg, J. Phys.: Condens. Matter **24**, 045004 (2012).

[29] I. Radovic, Lj. Hadzievski, and Z. L. Miskovic, Phys. Rev. B **77**, 075428 (2008).

[30] Kenneth W.-K. Shung, Phys. Rev. B **34**, 979 (1986).

[31] E. H. Hwang and S. Das Sarma, Phys. Rev. B **75**, 205418 (2007).

[32] Y. Barlas, T. Pereg-Barnea, M. Polini, R. Asgari, and A. H. MacDonald, Phys. Rev. Lett. **98**, 236601 (2007).

[33] K. F. Allison, D. Borka, I. Radovic, Lj. Hadzievski, and Z. L. Miskovic, Phys. Rev. B **80**, 195405 (2009).

[34] K. F. Allison and Z. L. Miskovic, Nanotechnology **21**, 134017 (2010).

[35] I. Radovic, D. Borka, and Z. L. Miskovic, Phys. Lett. A **375**, 3720 (2011).

[36] E. H. Hwang, R. Sensarma, and S. Das Sarma, Phys. Rev. B **82**, 195406 (2010).

[37] I. Radovic, V. Borka Jovanović, D. Borka, and Z. L. Miskovic, Nucl. Instrum. Methods Phys. Res., Sect. B **279**, 165 (2012).

[38] M. Alducin, V. M. Silkin, and J. I. Juaristi, Nucl. Instrum. Methods Phys. Res., Sect. B **256**, 383 (2007).

[39] V. M. Silkin, M. Alducin, J. I. Juaristi, E. V. Chulkov, and P. M. Echenique, J. Phys.: Condens. Matter **20**, 304209 (2008).

[40] D. Borka, I. Radovic, and Z. L. Miskovic, Nucl. Instrum. Methods Phys. Res., Sect. B **269**, 1225 (2011).

[41] V. Fessatidis, N. J. M. Horing, and A. Balassis, Phys. Lett. A **375**, 192 (2010).

[42] N. J. M. Horing and V. Fessatidis, IEEE Sens. J. **10**, 674 (2010).

[43] H. Winter, Phys. Rep. **367**, 387 (2002).

[44] Y.-H. Song, Y.-N. Wang, and Z. L. Miskovic, Phys. Rev. A **63**, 052902 (2001).

[45] Y.-H. Song, Y.-N. Wang, and Z. L. Miskovic, Phys. Rev. A **68**, 022903 (2003).

[46] Y.-N. Wang and Z. L. Miskovic, Phys. Rev. A **69**, 022901 (2004).

[47] D. J. Mowbray, Z. L. Miskovic, F. O. Goodman, and Y.-N. Wang, Phys. Rev. B **70**, 195418 (2004).

[48] G. Gumbs and A. Balassis, Phys. Rev. B **71**, 235410 (2005).

[49] D.-P. Zhou, Y.-N. Wang, L. Wei, and Z. L. Miskovic, Phys. Rev. A **72**, 023202 (2005).

[50] D. J. Mowbray, Z. L. Miskovic, and F. O. Goodman, Phys. Rev. B **74**, 195435 (2006).

[51] D. Borka, S. Petrovic, N. Neskovic, D. J. Mowbray, and Z. L. Miskovic, Phys. Rev. A **73**, 062902 (2006).

[52] D. Borka, D. J. Mowbray, Z. L. Miskovic, S. Petrovic, and N. Neskovic, Phys. Rev. A **77**, 032903 (2008).

[53] D.-P. Zhou, Y.-H. Song, Y.-N. Wang, and Z. L. Miskovic, Phys. Rev. A **73**, 033202 (2006).

[54] D. J. Mowbray, S. Chung, Z. L. Miskovic, and F. O. Goodman, Nanotechnology **18**, 424034 (2007).

[55] V. I. Shulga and P. Sigmund, Nucl. Instrum. Methods Phys. Res., Sect. B **88**, 97 (1994).

[56] Y.-N. Wang, Z. L. Miskovic, and W.-K. Liu, Phys. Rev. A **58**, 1287 (1998).

[57] Y.-H. Song, Y.-N. Wang, and Z. L. Miskovic, Phys. Rev. A **72**, 012903 (2005).

[58] Y. Susuki, H. Mukai, K. Kimura, and M. Mannami, Nucl. Instrum. Methods Phys. Res., Sect. B **48**, 347 (1990).

[59] Y. Susuki, T. Ito, K. Kimura, and M. Mannami, Phys. Rev. A **51**, 528 (1995).

[60] H. Winter, J. C. Poizat, and J. Remillieux, Nucl. Instrum. Methods Phys. Res., Sect. B **67**, 345 (1992).

[61] T. Bagdonata, M. Vicanek, J. I. Juaristi, and F. J. Garcia de Abajo, Nucl. Instrum. Methods Phys. Res., Sect. B **142**, 473 (1998).

[62] Y. Susuki, Phys. Rev. A **56**, 2918 (1997).

[63] I. Villó-Pérez, I. Abril, R. Garcia-Molina, and N. R. Arista, Phys. Rev. A **71**, 052902 (2005).

[64] I. Radovic, Lj. Hadzievski, N. Bibic, and Z. L. Miskovic, Phys. Rev. A **76**, 042901 (2007).

[65] S. Tomassone and A. Widom, Phys. Rev. B **56**, 4938 (1997).

[66] G. V. Dedkov and A. A. Kyasov, Nucl. Instrum. Methods Phys. Res., Sect. B **237**, 507 (2005).

[67] G. V. Dedkov and A. A. Kyasov, J. Phys.: Condens. Matter **20**, 354006 (2008).

[68] H. B. Nersisyan and A. K. Das, Phys. Rev. E **80**, 016402 (2009).

[69] J. M. Pitarke, V. M. Silkin, E. V. Chulkov, and P. M. Echenique, Rep. Prog. Phys. **70**, 1 (2007).

[70] D. J. Mowbray, S. Segui, J. Gervasoni, Z. L. Miskovic, and N. R. Arista, Phys. Rev. B **82**, 035405 (2010).

[71] N. D. Mermin, Phys. Rev. B **1**, 2362 (1970).

[72] M. V. Fischetti, D. A. Neumayer, and E. A. Cartier, J. Appl. Phys. **90**, 4587 (2001).

[73] S. Fratini and F. Guinea, Phys. Rev. B **77**, 195415 (2008).

[74] M. Ghaznavi, Z. L. Miskovic, and F. O. Goodman, Phys. Rev. B **81**, 085416 (2010).

[75] Y.-N. Wang, H.-T. Qiu, and Z. L. Miskovic, Phys. Rev. Lett. **85**, 1448 (2000).

[76] F. J. Garcia de Abajo and P. M. Echenique, Phys. Rev. B **48**, 13399 (1993).